Self-assembling proteins as high-performance substrates for embryonic stem cell self-renewal

Christopher J. Hill, Jennifer R. Fleming, Masoumeh Mousavinejad, Rachael Nicholson, Svetomir B. Tzokov, Per A. Bullough, Julius Bogomolovas, Mark R. Morgan, Olga Mayans[*] and Patricia Murray[*]

Dr C. J. Hill, M. Mousavinejad, R. Nicholson, Dr M. R. Morgan, Prof. P. Murray

Department of Cellular and Molecular Physiology, Institute of Translational Medicine, University of Liverpool, Nuffield Building, Crown Street, Liverpool L69 3BX, UK;

Dr J. R. Fleming, Prof. O. Mayans

Department of Biology, University of Konstanz, 78457 Konstanz, Germany;

Dr S. B. Tzokov, Prof. P. A. Bullough,

Department of Molecular Biology and Biotechnology, The Krebs Institute,

University of Sheffield, Sheffield S10 2TN, UK;

Dr J. Bogomolovas,

Department of Medicine, UCSD, La Jolla, California, USA;

Department of Cognitive and Clinical Neuroscience, Central Institute of Mental Health, Medical Faculty Mannheim, Heidelberg University, Germany.

Dr C. J. Hill, Prof. O. Mayans

Department of Biochemistry, Institute of Integrative Biology, University of Liverpool, Crown Street, Liverpool L69 7ZB, UK;

To whom correspondence should be addressed:

Prof. Patricia Murray, Tel: +44-151 794 5450, P.A.Murray@liverpool.ac.uk

Prof. Olga Mayans, Tel: +49-7531 882212, Olga.Mayans@uni-konstanz.de

* joint corresponding authors

The development of extracellular matrix (ECM) mimetics that imitate niche stem cell microenvironments and support cell growth for technological applications is intensely pursued. **Specifically, mimetics are sought that can enact control over the self-renewal and directed differentiation of human pluripotent stem cells (hPSCs) for clinical use. Despite considerable progress in the field, a major impediment to the clinical translation of hPSCs is the difficulty and high cost of large-scale cell production under xeno-free culture conditions using current matrices. Here, a bioactive, recombinant, protein-based polymer, termed ZT^{Fn}, is presented that closely mimics human plasma fibronectin and serves as an economical, xeno-free, biodegradable and functionally-adaptable cell substrate. The ZT^{Fn} substrate supports with high-performance the propagation and long-term self-renewal of human embryonic stem cells (hESC) while preserving their pluripotency. The ZT^{Fn} polymer can, therefore, be proposed as an efficient and affordable replacement for fibronectin in clinical grade cell culturing. Further, it can be postulated that the ZT polymer has significant engineering potential for further orthogonal functionalisation in complex cell applications.**

The generation of substrates that preserve pluripotency in human stem cells and direct their controlled differentiation is intensely pursued.[1,2] Such substrates are of critical value to stem cell-based applications, such as those concerning the modeling of disease, drug discovery, the screening of toxicants, and personalised therapies in regenerative medicine for conditions like age-related macular degeneration and Parkinson's disease.[3,4] Human pluripotent stem cells (hPSCs), specifically embryonic (hESCs) and induced pluripotent stem cells (iPSCs), are of critical significance in these pursuits.[5] Biomedical applications of hPSCs require large-scale *ex vivo* culture. Therapeutic uses require, in addition, xeno-free conditions to avoid risk of zoonotic transmission. Meeting these combined requirements is challenging as hPSCs are typically cultured on costly animal-derived substrates of undefined and variable batch-to-batch composition. In particular, hPSCs are commonly co-cultured with mouse fibroblast feeder cells or grown on Matrigel™, a complex mixture of ECM proteins secreted by mouse sarcoma cells that consists primarily of laminin, collagen IV and enactin.[6] Recently, substrates based on the recombinant eukaryotic expression of ECM proteins such as laminin or vitronectin have been introduced.[7,8] These successfully support hPSC self-renewal,[9–10] but have high purchase costs. Together with the expense of clinical grade culture media, this limits the up-scaling of hPSC expansion (e.g. in large-scale 3D culture systems using microcarriers[11]) using these substrates. Chemical substrates carrying conjugated peptides are also available, like Synthemax™. However, in addition to their high cost, their use in therapeutic applications could raise potential safety concerns. For example, Synthemax is made of carboxylic acid-carrying acrylate, to which peptides derived from vitronectin are attached using chemical cross-linking.[12] It successfully supports hPSC expansion[12] but it has been observed to lead to genetic abnormalities in long-term cell cultures.[13] In summary, the need for economic and safe translational materials persists.

The protein polymer ZT[14] holds promise to meet the need for an economical, homogeneous and functionally-adaptable cell substrate of controlled composition. ZT exploits the complexation of the protein telethonin (Tel) with the two N-terminal immunoglobulin (Ig) domains from titin, Z1Z2, which occurs naturally in human sarcomeres. Tel is "sandwiched" between two antiparallel Z1Z2 doublets, forming a robust intermolecular β-sheet that spans the three components[15] (**Figure 1a**). Both Tel and Z1Z2 can be overexpressed recombinantly in bacteria with a high yield. The ZT polymer is based on a Z1Z2-Z1Z2 fusion tandem (Z_{1212}) that causes the spontaneous propagative assembly of Z1Z2:Tel complexes.[14] ZT components can be readily functionalised by genetically encoding functional moieties into the building-blocks prior to their assembly. This strategy affords exact control on the position and stoichiometry of exogenous elements in the polymer. As proof of principle, ZT was engineered to display an affinity motif N-terminal to Tel that recruited gold nanoparticles to the polymer with nano-scale periodicity.[14] Moreover, the isolated Z1 domain showed that its CD loop permits the grafting of lengthy peptide motifs without causing fold perturbations, serving as an accessible and functional epitope.[16] Thereby, the ZT polymer can allow the incorporation of functional moieties in a controllable fashion.

Here, we aimed to exploit the polymeric nature, scaffolding capabilities and ease of production of the ZT polymer to develop an economic substrate for culturing hESCs. Specifically, we aimed to mimic the efficiency of human fibronectin in supporting hESC self-renewal in serum-free conditions.[17,18] In fibronectin, the small peptide RGD in domain Fn10, is the critical integrin-binding motif mediating cell adhesion, spreading, and migration.[19] Accordingly, RGD peptide mimetics are frequently employed as adhesive moieties on substrates for cell culture applications.[20,21] hESCs do not attach to RGD peptides,[18] but a proteolytic 120 kDa fibronectin fragment containing the complete Fn10 domain successfully

supported their self-renewal.[18] Building on this knowledge and on the fact that fibronectin supports cell attachment with higher efficacy than RGD alone[22], we have assessed the mimetic potential of the ZT polymer functionalised with RGD and Fn10 moieties.

Firstly, we established that the ZT polymer remains unaltered upon display of exogenous bioreactive motifs. For this, we created two functionalised Z_{1212} variants by genetically fusing DNA sequences: (1) a Z_{1212} tandem carrying the fibronectin GRGDS motif in the CD loop of the second Z1 domain (Z_{1212}^{RGD}) (**Figure 1a,b**) and (2) a Z_{1212} chimera where the Fn10 domain from fibronectin had been fused C-terminally to the tandem (Z_{1212}^{Fn}) via the same GETTQ linker sequence originally used to join Z1Z2 doublets[14] (**Figure 1c**). In Z_{1212}^{RGD}, the GRGDS sequence has higher affinity for integrins than the core RGD motif alone, with the flanking residues known to enhance cell attachment.[23,24] This resulted ultimately in the substitution of four native Z1 residues for a seven-residue peptide (**Figure 1b**). For comparison, a biologically inactive RGE version[22] was created (Z_{1212}^{RGE}).

The variants Z_{1212}^{RGD}, Z_{1212}^{RGE} and Z_{1212}^{Fn} proved undemanding to produce recombinantly in *E. coli* cultures. Pure, stable, and monodisperse samples of all variants were produced in high yields equivalent to the wild type protein Z_{1212} (>40 mg/L culture) (**Figure S1a,b** in Supporting Information). To test the capability of the variants to self-assemble, and given that the Z1Z2/Tel complex is the fundamental assembly unit of the ZT polymer, we considered that complexation of Tel by modified Z1Z2 samples at the native 2:1 ratio was evidence of undisrupted assembly in these variants. Therefore, we produced Z1Z2^{RGD}/Tel and Z1Z2^{Fn}/Tel complexes by *in cellulo* co-expression, studied their migration in SEC and measured their MM by SEC-MALLS, confirming the expected 2:1 association (**Figure S1c-e** in Supporting Information). Next, we mixed the polymerising Z_{1212} variants (Z_{1212}^{RGD}, Z_{1212}^{RGE}

and $Z_{1212}{}^{Fn}$) with Tel and confirmed assembly by native-PAGE (**Figure S1f,g** in Supporting Information) and electron microscopy (**Figure 1d**); the resulting polymers are here denoted ZT^{RGD}, ZT^{RGE} and ZT^{Fn}, respectively. Taken together, these results proved that the Z_{1212} building block could be successfully functionalised in both internal (CD loop) and external (C-terminus) positions, maintaining its structural integrity and its polymerisation capability.

The conformation of the RGD motif influences the selectivity and affinity of the integrin receptors it engages and, thereby, its efficiency in cell adhesion.[22,24–26] Thus, we studied whether the RGD motif inserted in Z1 resembles the motif in the native Fn10. In Fn10, the motif is located within the FG β-hairpin loop that resembles a distorted type II' β-turn with high intrinsic flexibility.[25,27] To confirm the degree of structural mimicry achieved by the loop engineered in Z1, we elucidated the crystal structure of $Z_{1212}{}^{RGD}$ at 3.0 Å resolution (**Table S1** in Supporting Information). The structure confirmed that the fold of Z1 is not altered by the inserted sequence, with the structure closely matching that of wild-type Z1 (rmsd=0.47 Å to Z1 in PDB entry 2A38[28]) (**Figure 1e**). The inserted SSGRGDSS sequence formed a loop protruding from the surface of Z1 as expected, in quasi β-turn conformation and with evident signs of flexibility (**Figure S2** in Supporting Information), thereby reproducing the features of the native motif in fibronectin. Comparison of crystal structures for modified Z1 and Fn10 (PDB IDs: 1FNA, 1FNF, 4MMX) showed that the engineered RGD motif locally adopts a similar conformation (**Figure 1f,g**). These data confirm the ability of the introduced sequence to emulate the native RGD motif.

We then tested whether the functionalised ZT polymer promoted spreading of murine mesenchymal stromal cells (mMSCs) by comparing the relative efficiency of cell attachment to the ZT^{RGD} and ZT^{Fn} polymers. For this analysis, we employed the clonally-derived mMSC

line D1, which tolerates a variety of RGD-based substrata.[29–31] We cultured mMSCs on non-adhesive polystyrene plates coated with the ZT^{RGD}, ZT^{RGE} and ZT^{Fn} polymers under serum-free conditions and quantified cell attachment and dispersion. At 2h culture, mMSCs showed adherence to both ZT^{RGD} and ZT^{Fn} in a concentration-dependent manner, confirming the accessibility of both RGD and Fn10 moieties within the polymer (**Figure 2a,b**). However, consistently more cells attached to ZT^{Fn} than to ZT^{RGD}. As expected, the non-bioactive ZT^{RGE} did not support cell attachment. mMSC spreading was quantified by calculating the average cell area for all conditions (**Figure 2c**). Spreading was significantly increased on ZT^{RGD} and ZT^{Fn} compared to the plastic control, but ZT^{Fn} showed the best performance. In addition, cell profiles were used to determine the average circularity (or area-to-perimeter ratio), aspect ratio (AR) and solidity of mMSCs plated on human plasma fibronectin, ZT^{RGD} or ZT^{Fn} (**Figure 2d**). Values were remarkably equivalent for cells grown on ZT^{Fn} or fibronectin, while differences were observed in cells plated on ZT^{RGD}. Higher circularity and solidity values for mMSCs cultured on ZT^{RGD} correlated with a symmetric spreading on this substrate, whilst the higher AR and lower solidity of cells cultured on ZT^{Fn} or fibronectin indicate anisotropic spreading. By using a competitive inhibition assay that employed a linear GRGDS peptide, we confirmed that the observed effects on cell attachment are due to the respective specificities of the engineered ZT^{RGD} and ZT^{Fn} polymers for integrin binding (**Figure S3** in Supporting Information). To further investigate attachment, we examined the impact of the different substrates on cytoskeletal organisation and adhesion complexes (**Figure 2e**). Focal complexes were observed on all substrates. However, mMSCs plated on fibronectin or ZT^{Fn} displayed well developed stress fiber networks, whilst cells attached to ZT^{RGD} exhibited fewer stress fibers and a cortical actin distribution. Taken together, cell adhesion and spreading data indicated that the loop-grafted GRGDS motif was insufficient to support effective mMSC

attachment, but that the interaction of cells with the ZT^{Fn} polymer mimicked that of full-length human fibronectin.

To assess the capability of ZT^{Fn} to support cell growth in potential clinical applications, we then tested this polymer on human HUES7 cells, proving that hESCs attach to and proliferate on ZT^{Fn}. HUES7 cells neither attach nor spread on materials functionalised with RGD peptides, but they can be cultured on fibronectin or large proteolytic fragments thereof.[18] Accordingly, we confirmed that HUES7 cells did not adhere to ZT^{RGD} (**Figure 2f**) or to the Fn10 domain alone (in the absence of the polymerised ZT) (**Figure S4** in Supporting Information). However, they attached successfully to the ZT^{Fn} polymer. Moreover, the extent of HUES7 cell attachment and spreading on ZT^{Fn} was comparable to that on human plasma fibronectin (both substrates used at comparable amounts; **Figure S5** in Supporting Information). Cell attachment and spreading on both fibronectin and ZT^{Fn} were only moderately lower than those obtained from the complex matrix Matrigel™ (**Figure 2g**). We concluded that the ZT^{Fn} polymer comparatively resembled the performance of native fibronectin in supporting hESCs growth and spread.

We further compared the effect of ZT^{Fn}, fibronectin and Matrigel™ on cell growth. As our long-term goal is to support the clinical application of hPSC, we focused this test on established biological substrates, naturally produced by living cells and composed only of biodegradable, folded protein components that have not undergone any chemical treatment. We did not employ chemical substrates (e.g. Synthemax™) as comparative controls to ZT^{Fn} because of their more distant composition. The results showed that whilst average cell circularity and solidity were consistent between substrates, the average AR of cells plated on ZT^{Fn} was significantly higher than that of cells cultured on fibronectin and particularly higher

8

than Matrigel™, reflecting the asymmetric spreading on ZT^{Fn} (**Figure 2h**). F-actin and paxillin staining showed that focal adhesions were present in HUES7 cells grown on Matrigel™ and ZT^{Fn}, but were less common on fibronectin (**Figure 2i**). Filopodia-like projections were abundant in cells cultured on Matrigel™ and in some cells grown on fibronectin, but cells grown on ZT^{Fn} lacked projections and exhibited a geometric morphology with well-defined actin stress fibers (**Figure 2i**). Intriguingly, the observed increase in actin filamentation was sustained following prolonged culture on ZT^{Fn} (**Figure S6a** in Supporting Information). Despite their morphological differences, cells grown on ZT^{Fn} retained an ESC phenotype following single cell dissociation as confirmed by nuclear OCT4 and NANOG expression (**Figure S6b** in Supporting Information). Cells on all substrates successfully began to form colonies after 24 h (**movies S1, S2 & S3**) and robustly expressed pluripotency markers (**Figure S7a** in Supporting Information). Additionally, focal adhesions were found to contain focal adhesion kinase (FAK) phosphorylated at tyrosine 397 (pY397), confirming the activation of signalling pathways downstream of integrin engagement (**Figure S7b** in Supporting Information).

To better characterise the molecular mode of action of ZT^{Fn}, we set to identify the integrins it engages. As fibronectin attachment is largely dependent on α5β1 and αVβ3[32], we tested first the involvement of these integrins in HUES7 cells plated on ZT^{Fn}. Whilst we detected α5β1 in focal adhesions (**Figure 3a**), we did not detect αVβ3 (**Figure S8a,b** in Supporting Information). Unexpectedly, targeting the αV subunit alone produced robust focal adhesion-like staining, as did an antibody against subunit β5 unique to the αVβ5 heterodimer (**Figure 3b**). Thus, we concluded that HUES7 cell attachment to ZT^{Fn} is mediated by αVβ5 and α5β1 integrins present in cell adhesion complexes (**Figure 3c**). After two days of culture, the cells continued to engage αVβ5 (**Figure S9** in Supporting Information). On the contrary,

cells grown on Matrigel™ and fibronectin were negative for both αV and β5 adhesion-specific staining (**Figure S8b** in Supporting Information). Currently, there is no robust evidence for the binding of αVβ5 to fibronectin, therefore its engagement by ZT^{Fn} was unexpected. Integrin αVβ5 is a well characterised receptor of the RGD motif in the somatomedin-B domain from vitronectin.[33,34] Accordingly, αVβ5 mediates hPSC attachment to vitronectin,[35,36] and attachment of hiPSC lines IMR90 and Gibco episomal line to the synthetic vitronectin-based peptide acrylate, Synthemax™.[9] In agreement with our finding, we observed that the morphology of cells grown on ZT^{Fn} strikingly emulated that of cells grown on vitronectin (**Figure S10** in Supporting Information). Both cells cultured on vitronectin and ZT^{Fn} also displayed increased stress fiber formation and large focal adhesions containing FAK pY397 (**Figure S10** in Supporting Information). The larger size of focal adhesions formed on the ZT^{Fn} substrate, caused the cells to migrate more slowly in comparison to Matrigel™ and fibronectin substrates, as a close relationship exists between the size of focal adhesions and cell migration speed (**Figure 3d**).[37] Slow migration, was reproduced by cells cultured on vitronectin (**Figure 3d**). Upon prolonged culture on all substrates, cells formed colonies. Colonies grown on Matrigel^{TM} exhibited α5β1 expression in distinct fibrillar patterns whilst expression of this integrin was lost on ZT^{Fn} (**Figure S9a** in Supporting Information). Yet, colonies grown on ZT^{Fn} continued to express αVβ5 (**Figure S9b** in Supporting Information). It is remarkable to observe that the presentation of the Fn10 domain in the context of the ZT^{Fn} polymer induces a preferential switch to αVβ5. It can be concluded that not only the chemical composition of the bioreactive motif but the geometry of its presentation to the cell is critical for integrin selectivity. This finding adds to the previous observation that the specific conformation of fibronectin on different synthetic surfaces dramatically influenced integrin binding.[38]

To investigate whether the observed difference in integrin engagement affected cell phenotype, we assessed the ability of ZT^{Fn} to promote survival of single HUES7 cells. We found that hESCs maintain a pluripotent phenotype following prolonged culture on ZT^{Fn}, which supported clonal expansion with an efficacy comparable to fibronectin and only moderately reduced relative to Matrigel™ (**Figure 4a**). Cell proliferation was somewhat reduced on ZT^{Fn} compared to Matrigel™, but was not significantly different from fibronectin (**Figure 4b**). Finally, we assessed the ability of ZT^{Fn} to maintain the long-term self-renewal of HUES7 cells. For this, the cells were cultured in mTeSR1 medium (without ROCK inhibitor, a compound used to extend cell survival[39]) for up to 18 passages. The cells were passaged every 5-6 days as clumps containing 50-200 cells; they were cultured on ZT^{Fn} for approx. 4 months in total with no noticeable negative effects. The cells grew as colonies with typical morphologies, including a high nuclear-to-cytoplasmic ratio and prominent nucleoli. Cells also retained nuclear expression of OCT4 and NANOG (**Figure S11a** in Supporting Information). Relative gene expression analysis of pluripotency markers *OCT4*, *NANOG* and *SOX2* was used to compare cells cultured on Matrigel™ with those cultured on fibronectin or ZT^{Fn} for 1, 5 and 10 passages. *NANOG* and *SOX2* transcript levels were found to be significantly decreased in cells cultured on fibronectin at passage 10 (**Figure 4c**). Although *NANOG* expression was also downregulated in cells cultured on ZT^{Fn} at passage 10 relative to Matrigel™, expression was significantly higher compared to fibronectin (**Figure 4c**). Cells cultured on ZT^{Fn} or fibronectin for 13 passages were used to form embryoid bodies that contained derivatives of the three embryonic germ layers *in vitro* (**Figure S11b** in Supporting Information). Positive staining for Brachyury (mesoderm), GATA6 (GATA-binding factor 6, endoderm) and Nestin (ectoderm) confirmed that HUES7 cells remained pluripotent following their long-term culture on ZT^{Fn}.

In conclusion, we show that the ZT polymer is a chimeric composite of recombinant human proteins, with high functionalisation capability.[14] Neither loop grafting nor domain fusion reduced the bacterial production yield of Z_{1212} variants, an important consideration for large scale applications. We show that the functionalised ZT system is compatible with standard cell culture techniques and that it serves as an efficient substrate for the long-term self-renewal of pluripotent hESCs, being a viable substitute for natural fibronectin and other commonly used matrices for hPSC culture. The material is produced in bacteria, it is scalable and predictably compatible with 3D-culture systems. In this regard, the incorporation of natural ECM proteins with 3D-materials using cross-linking is established in the bibliography. For example, fibronectin has been photo-crosslinked into hyaluronic acid 3D-hydrogels for endothelial cell culture.[40] As the ZT polymer is composed of folded protein domains that closely resemble those of fibronectin, its incorporation in 3D-systems via chemical cross-linking can be expected to be an equally feasible goal. In summary, economical substrates of controlled composition such as the ZT^{Fn} polymer will be essential for further advancement in the clinical translation of PSC-based therapies.

Supporting Information

Supporting Information is available from the Wiley Online Library or from the authors.

Author contributions

C.J.H., O.M. and P.M. conceived the study. C.J.H., O.M., M.R.M. and P.M. designed experiments. C.J.H. and J.B. performed molecular cloning. C.J.H produced and characterised protein constructs and assemblies. C.J.H., S.B.T. and P.A.B. carried out electron microscopy studies. C.J.H., J.R.F. and O.M. analysed protein structure. C.J.H., M.M. and R.N. performed cell-based experiments and data analysis. C.J.H. performed confocal imaging. C.J.H., O.M., P.M. and M.R.M. wrote the manuscript.

Competing interests

The authors declare competing financial interests: C.J.H., O.M. and P.M. disclose a pending patent on the use of Fn10 as a chimeric fusion protein of the ZT system.

Data availability

The coordinates and X-ray diffraction data for the crystal structure of Z_{1212}^{RGD} have been deposited with the Protein Data Bank (www.rcsb.org) with accession code 6FWX.

References

[1]   C. M. Madl, S. C. Heilshorn, *Annu. Rev. Biomed. Eng.* **2018**, *20*, annurev.

[2]   Z. Liu, M. Tang, J. Zhao, R. Chai, J. Kang, *Adv. Mater.* **2018**, 1705388.

[3]   R. S. Thies, C. E. Murry, *Development* **2015**, *142*, 3614.

[4]   Y. Avior, I. Sagi, N. Benvenisty, *Nat. Rev. Mol. Cell Biol.* **2016**, *17*, 170.

[5]   Y. Shi, H. Inoue, J. C. Wu, S. Yamanaka, *Nat. Rev. Drug Discov.* **2017**, *16*, 115.

[6]   C. S. Hughes, L. M. Postovit, G. A. Lajoie, *Proteomics* **2010**, *10*, 1886.

[7]   E. Sanjar, S. Jin, *World J. Stem Cells* **2015**, *7*, 243.

[8]   Y. Fan, J. Wu, P. Ashok, M. Hsiung, E. S. Tzanakakis, *Stem Cell Rev. Reports* **2015**, *11*, 96.

[9]   S. Jin, H. Yao, J. L. Weber, Z. K. Melkoumian, K. Ye, *PLoS One* **2012**, *7*, DOI 10.1371/journal.pone.0050880.

[10]   B. O. Pennington, D. O. Clegg, Z. K. Melkoumian, S. T. Hikita, *Stem Cells Transl. Med.* **2015**, *4*, 165.

[11]   C. Kropp, D. Massai, R. Zweigerdt, *Process Biochem.* **2017**, *59*, 244.

[12]   Z. Melkoumian, J. L. Weber, D. M. Weber, A. G. Fadeev, Y. Zhou, P. Dolley-Sonneville, J. Yang, L. Qiu, C. A. Priest, C. Shogbon, A. W. Martin, J. Nelson, P. West, J. P. Beltzer, S. Pal, R. Brandenberger, *Nat. Biotechnol.* **2010**, *28*, 606.

[13]   J. W. Lambshead, L. Meagher, J. Goodwin, T. Labonne, E. Ng, A. Elefanty, E. Stanley, C. M. O'Brien, A. L. Laslett, *Sci Rep.* **2018**, *8*, 701.

[14]   M. Bruning, L. Kreplak, S. Leopoldseder, S. A. Muller, P. Ringler, L. Duchesne, D. G. Fernig, A. Engel, Z. Ucurum-Fotiadis, O. Mayans, *Nano Lett.* **2010**, *10*, 4533.

[15]   P. Zou, N. Pinotsis, S. Lange, Y.-H. Song, A. Popov, I. Mavridis, O. M. Mayans, M. Gautel, M. Wilmanns, *Nature* **2006**, *439*, 229.

[16]   M. Bruning, I. Barsukov, B. Franke, S. Barbieri, M. Volk, S. Leopoldseder, Z. Ucurum, O. Mayans, *Protein Eng. Des. Sel.* **2012**, *25*, 205.

[17]   M. A. Baxter, M. V. Camarasa, N. Bates, F. Small, P. Murray, D. Edgar, S. J. Kimber, *Stem Cell Res.* **2009**, *3*, 28.

[18]   D. M. Kalaskar, J. E. Downes, P. Murray, D. H. Edgar, R. L. Williams, *J. R. Soc. Interface* **2013**, *10*, 20130139.

[19]   A. J. Zollinger, M. L. Smith, *Matrix Biol.* **2017**, *60–61*, 27.

[20]   S. Macneil, S. Rimmer, L. Perlin, S. Rimmer, S. Macneil, S. Rimmer, *Soft Matter* **2008**, *4*, 2331.

[21]   S. L. Bellis, *Biomaterials* **2011**, *32*, 4205.

[22]   A. Hautanen, J. Gailit, D. M. Mann, E. Ruoslahti, *J. Biol. Chem.* **1989**, *264*, 1437.

[23]   M. D. Pierschbacher, E. Ruoslahti, *Nature* **1984**, *309*, 30.

[24]   T. G. Kapp, F. Rechenmacher, S. Neubauer, O. V. Maltsev, E. A. Cavalcanti-Adam, R.

Zarka, U. Reuning, J. Notni, H. J. Wester, C. Mas-Moruno, J. Spatz, B. Geiger, H. Kessler, *Sci. Rep.* **2017**, *7*, 39805.

[25] D. J. Leahy, I. Aukhil, H. P. Erickson, *Cell* **1996**, *84*, 155.

[26] E. Ruoslahti, B. Obrink, *Exp. Cell Res.* **1996**, *227*, 1.

[27] A. L. Main, T. S. Harvey, M. Baron, J. Boyd, I. D. Campbell, *Cell* **1992**, *71*, 671.

[28] M. Marino, P. Zou, D. Svergun, P. Garcia, C. Edlich, B. Simon, M. Wilmanns, C. Muhle-Goll, O. Mayans, *Structure* **2006**, *14*, 1437.

[29] N. Huebsch, P. R. Arany, A. S. Mao, D. Shvartsman, O. A. Ali, S. A. Bencherif, J. Rivera-Feliciano, D. J. Mooney, *Nat. Mater.* **2010**, *9*, 518.

[30] Y. Lei, S. Gojgini, J. Lam, T. Segura, *Biomaterials* **2011**, *32*, 39.

[31] M. Mehta, C. M. Madl, S. Lee, G. N. Duda, D. J. Mooney, *J. Biomed. Mater. Res. - Part A* **2015**, *103*, 3516.

[32] M. R. Morgan, A. Byron, M. J. Humphries, M. D. Bass, *IUBMB Life* **2009**, *61*, 731.

[33] J. P. Kim, K. Zhang, J. D. Chen, R. H. Kramer, D. T. Woodley, *J Biol Chem* **1994**, *269*, 26926.

[34] I. Schvartz, D. Seger, S. Shaltiel, *Int. J. Biochem. Cell Biol.* **1999**, *31*, 539.

[35] S. R. Braam, L. Zeinstra, S. Litjens, D. Ward-van Oostwaard, S. van den Brink, L. van Laake, F. Lebrin, P. Kats, R. Hochstenbach, R. Passier, A. Sonnenberg, C. L. Mummery, *Stem Cells* **2008**, *26*, 2257.

[36] T. J. Rowland, L. M. Miller, A. J. Blaschke, E. L. Doss, A. J. Bonham, S. T. Hikita, L. V. Johnson, D. O. Clegg, *Stem Cells Dev.* **2010**, *19*, 1231.

[37] D. H. Kim, D. Wirtz, *FASEB J.* **2013**, *27*, 1351.

[38] B. G. Keselowsky, D. M. Collard, A. J. García, *J. Biomed. Mater. Res. Part A* **2003**, *66A*, 247.

[39] K. Watanabe, M. Ueno, D. Kamiya, A. Nishiyama, M. Matsumura, T. Wataya, J. B. Takahashi, S. Nishikawa, S. Nishikawa, K. Muguruma, Y. Sasai, *Nat. Biotechnol.* **2007**, *25*, 681.

[40] S. K. Seidlits, C. T. Drinnan, R. R. Petersen, J. B. Shear, L. J. Suggs, C. E. Schmidt. *Acta Biomater*. **2011**, *7*, 2401.

Figure Legends

Figure 1. The functionalised ZT polymer. (**A**) Crystal structure of the "sandwich" complex formed by two antiparallel Z1Z2 Ig-doublets from titin (blue) and Tel (red) (PDB: 1YA5[15]). The CD loop of domain Z1 is boxed. (**B**) Sequence of the native and modified CD loop. The residues introduced are coloured red. (**C**) Z_{1212} protein carrying a C-terminally fused domain Fn10 from human fibronectin (PDB: 1FNF[25], green). Fusion of naturally-occurring protein moieties in this chimera uses a GETTQ linker sequence. The native RGD motif located within the FG loop of Fn10 is displayed. (**D**) Transmission electron micrographs of ZT^{WT}, ZT^{RGD}, ZT^{RGE} and ZT^{Fn} polymers post-assembly (scale bars correspond to 100 nm). (**E**) Crystal structure of the GRGDS modified Z1 domain superimposed on wild-type Z1 (PDB 2A38[28]). (**F**) Superimposition of crystal structures of domain Fn10 from fibronectin (PDB codes are given). The conformational flexibility of the RGD loop (coloured) is manifest. (**G**) Superimposition of the RGD loop in Z1 (orange) with those from Fn10 structures shows that the motif incorporated in Z1 adopts a near-native conformation at the local level (structure 1FNA is excluded as its conformation is unique).

Figure 2. Murine MSC and human ESC adhesion and spreading on ZT substrates. (**A**) Representative phase-contrast micrographs of mMSCs cultured for 2h under serum-free conditions on non-treated plastic coated with ZT polymers at 10 μg/mL (scale bar = 100 μm). (**B**) Effect of ZT^{RGE} (non-bioactive), ZT^{RGD} and ZT^{Fn} substrates on mMSC adhesion and (**C**) spreading. Cell attachment is expressed as a percentage of the positive control (fibronectin at 10 μg/mL) that was taken as 100%. The average area of cells grown on fibronectin is included for comparison. Statistical significance in b. and c. is in reference to a non-treated surface (0 μg/mL). (**D**) Comparisons of the average circularity, aspect ratio and solidity of cells grown on

16

non-treated plastic coated with fibronectin, ZT^{RGD} or ZT^{Fn}, all samples at 10 µg/mL. (**E**) Representative confocal micrographs of cells stained for F-actin (green), paxillin (red) and DAPI (blue) following attachment to different substrates. Zooms of boxed areas are shown in the upper right of the respective image. (**F**) Representative phase-contrast images of HUES7 cells cultured for 2 and 4h on ZT^{RGD}, ZT^{Fn} and control substrates. Scale bar = 100 µm. (**G**) Quantification of cell attachment and spreading is shown by the bar charts. Cell attachment is expressed as a percentage of the positive control (Matrigel™) that was taken as 100%. (**H**) Comparisons of the average circularity, aspect ratio and solidity of cells plated on plastic plates coated with Matrigel™, fibronectin or ZT^{Fn} at 10 µg/mL. (**I**) Representative confocal micrographs of cells stained for F-actin (green), paxillin (red) and DAPI (blue) following attachment to different substrates. Zooms of boxed areas are shown in the upper right of the respective image. (Error bars represent SEM, n=3. Scale bar = 50 µm if not otherwise stated. Throughout, $*p < 0.05$, $**p < 0.01$ and $***p<0.001$).

Figure 3. Integrin engagement and migration of human ESCs on ZT^{Fn}. (**A**) Representative pseudo-coloured confocal micrographs show paxillin (red) and α5 integrin subunit (green) co-staining of HUES7 cells following 4h culture on ZT^{Fn}. The fluorescence intensity linescan profile was generated from the merged image shown below. Scale bars = 10 µm. (**B**) Staining of αV and β5 integrin subunits (red). The merged images show counterstaining for F-actin (green) and DAPI (blue). Scale bar = 50 µm. (**C**) Pseudo-coloured micrographs show co-staining of α5 (green) and β5 (purple) subunits in HUES7 cells cultured on ZT^{Fn}. A fluorescence intensity profile is shown for the merged image. Scale bars = 10 µm. (**D**) Box-and-whisker plots of cell migration. Boxes show the median (*middle line*), mean (*square*), 25th and 75th percentiles (*box ends*) and 5th and 95th percentiles (*whiskers*) (*n*=80).

Figure 4. Human ESC clonal culturing and self-renewal on ZT^{Fn}. (**A**) Clonogenic survival of cells plated on Matrigel™, fibronectin and ZT^{Fn} at a density of 2.5 x 10^3/cm^2. (**B**) Proliferative capacity of HUES7 cells cultured on Matrigel™, fibronectin or ZT^{Fn} over 4 days. Error bars represent SEM (n=4). (**C**) Quantitative RT-qPCR analysis of *NANOG*, *OCT4* and *SOX2* expression levels in HUES7 cells cultured on fibronectin or ZT^{Fn} for one, five and ten passages relative to cells cultured on Matrigel™. Error bars represent SEM (n=3).

Figures

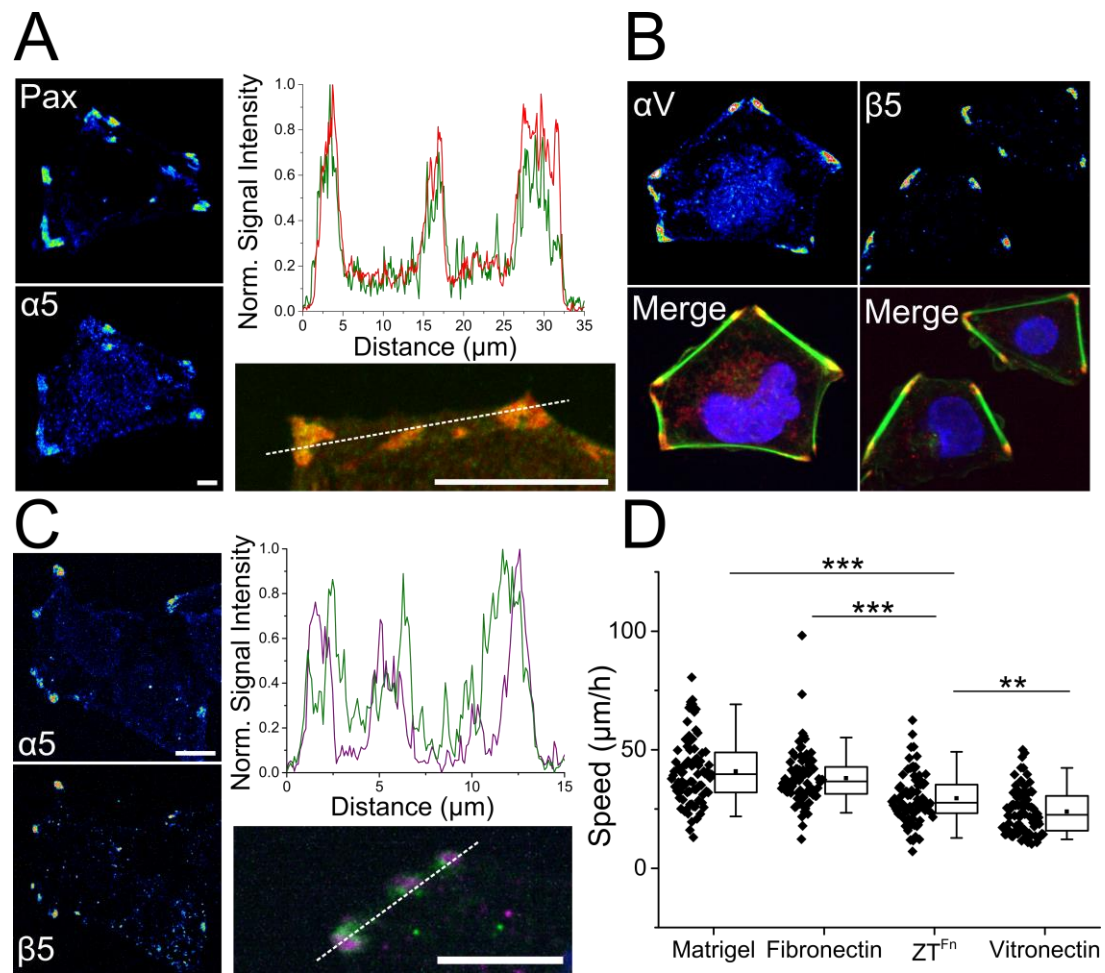## Figure 1.
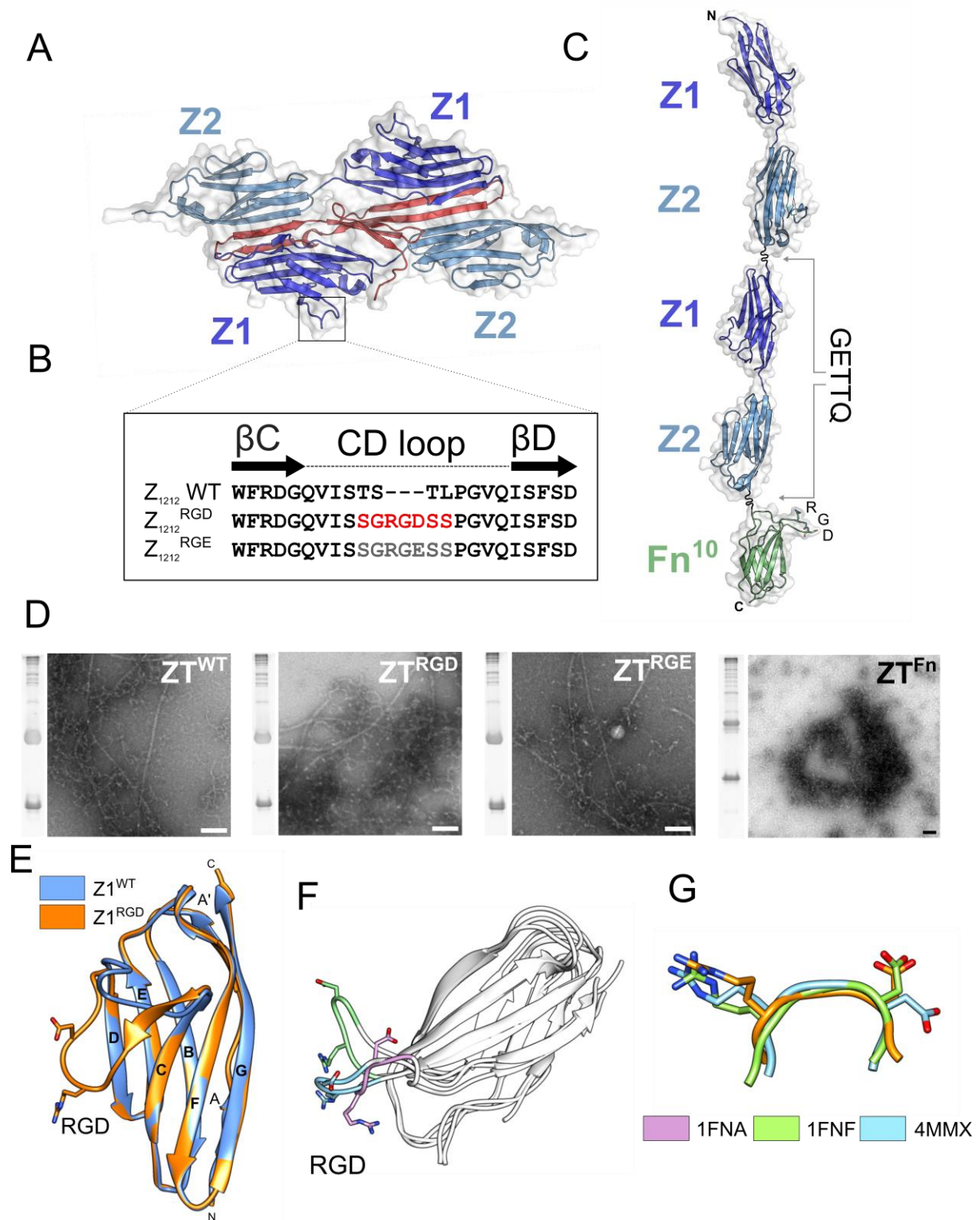
Figure 2.

Figure 3.

Figure 4.

A. Cloning Efficacy (%) for Matrigel, Fibronectin, ZT^{Fn}. ** and $p = 0.55$.

B. Absorbance 440 nm vs Time (hours) for Matrigel, Fibronectin, ZT^{Fn}. * and $p = 0.07$.

C. Relative Gene Expression for NANOG, OCT4, SOX2 across P1, P5, P10 for Fibronectin and ZT^{Fn}. NANOG $p = 0.005$, ***, **. SOX2 **.
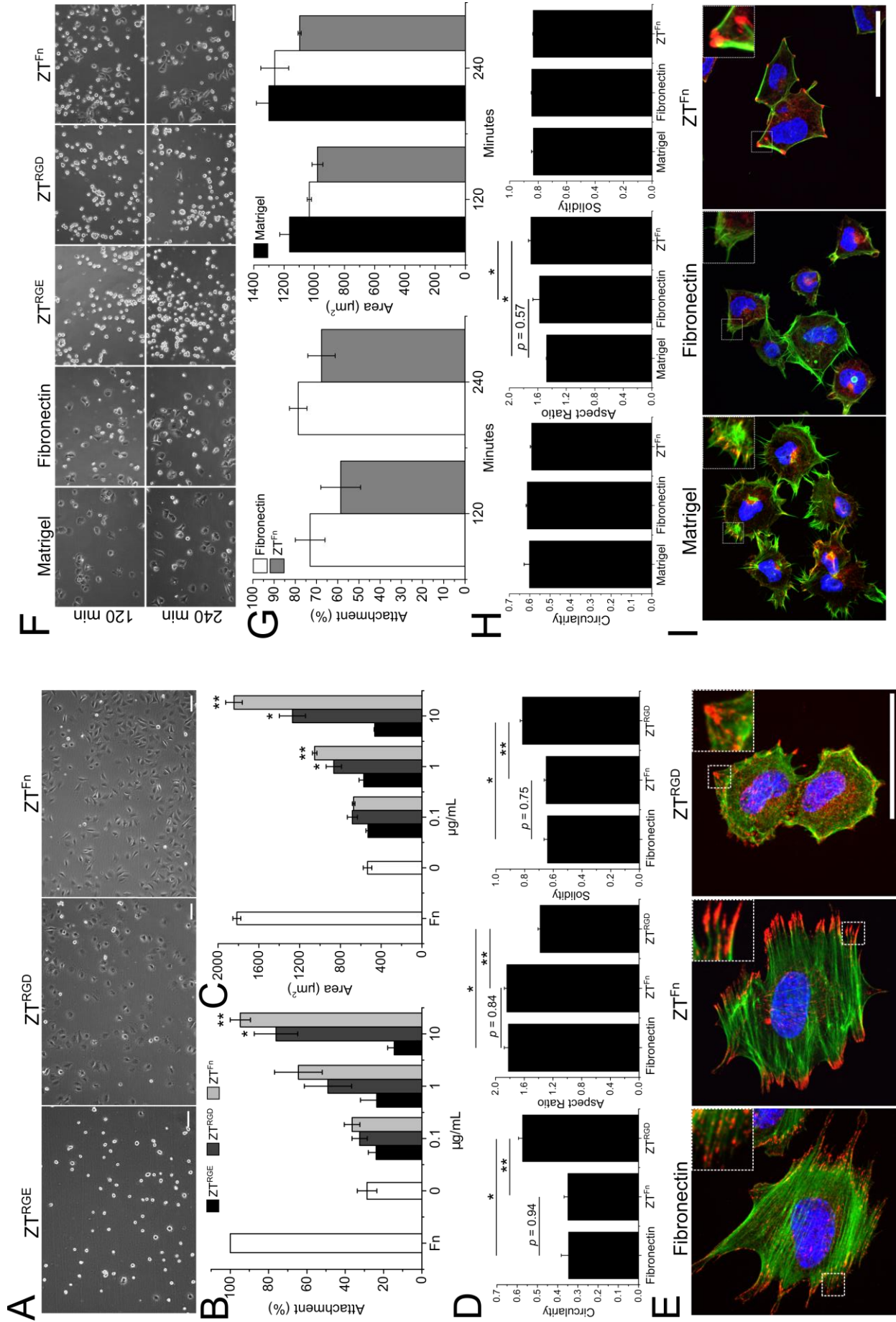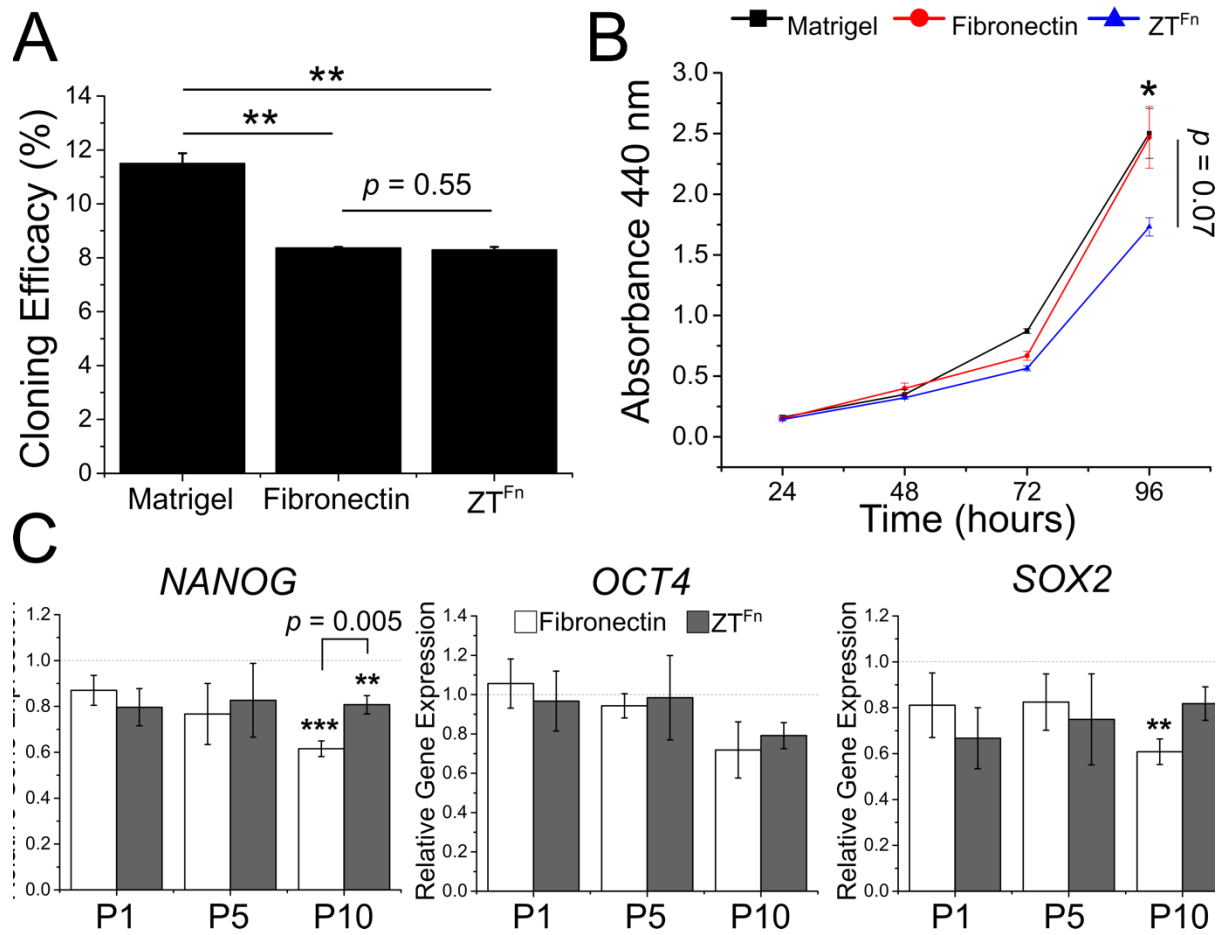
Supplementary Information

Self-assembling proteins as high-performance substrates for embryonic stem cell self-renewal

Christopher J. Hill, Jennifer R. Fleming, Masoumeh Mousavinejad, Rachael Nicholson, Svetomir B. Tzokov, Per A. Bullough, Julius Bogomolovas, Mark R. Morgan, Olga Mayans,[*] and Patricia Murray[*]

Experimental Section

Cloning

The Z_{1212} and cysteine-null truncated telethonin proteins have been previously described.[1] Variant Z_{1212}^{RGD} was created by inserting the RGD motif into the CD loop of the second Z1 domain between residues 46 and 51 (UniProt Q8WZ42) using overlap extension PCR. The grafted insert was seven amino acids long (SGRGDSS) and replaced residues 47-50 of Z1. Variant Z_{1212}^{RGE} was generated from Z_{1212}^{RGD} using QuikChange[2]. For the generation of Z_{1212}^{Fn}, the region of human fibronectin encoding FnIII domains 8 to 11 (residues 1269-1638; UniProt P02751) was amplified from human cDNA and used for subcloning. Domain Fn10 (residues 1448-1543) was amplified from the latter fragment with specific primers encoding

for restriction sites. A fusion protein consisting of Z_{1212} carrying domain Fn10 joined C-terminally was created as follows: the sequence encoding Fn10 was amplified with an N-terminal BbsI restriction site incorporated by the forward primer; a Z_{1212} amplicon with a C-terminal BbsI site was made in the same fashion and both fragments were ligated after digestion. Primers were designed to introduce a GETTQ linker sequence between the last residue of Z_{1212} (Q389) and the start residue of Fn10 (S1448). All constructs were confirmed by sequencing and cloned into the pETM-11 vector (EMBL) to generate a His_6-tagged protein product with a TEV protease cleavage site. For co-expression with telethonin, the Ig-doublet Z1Z2 from human titin (residues 1-196; Q8WZ42) containing the engineered RGD motif in Z1 (described above) or fused to Fn10 was subcloned from the respective Z_{1212} variants and inserted into the vector pET-15b (Novagen) to exclude the N-terminal His_6-tag. The resulting construct could only be purified by affinity chromatography when bound to telethonin.

Protein expression and purification

Recombinant proteins were expressed in *E. coli* BL21(DE3) (Novagen). Bacterial cells were cultured at 37°C to an OD_{600} of 0.6 in Luria Bertani medium supplemented with 25 μg/mL kanamycin or 50 μg/mL ampicillin for constructs encoded by pETM-11 or pET-15b vectors, respectively. Protein expression was induced using 1mM isopropyl-thio-β-D-galactopyranoside (IPTG) and cultures were grown further overnight at 18°C. Cells were harvested by centrifugation. Isolation of telethonin from inclusion bodies was as described.[1] For Z_{1212} and its variants, cell pellets were resuspended in lysis buffer (50 mM Tris-HCl pH 7.4, 300 mM NaCl) supplemented with a protease inhibitor cocktail (Roche) and 10 μg/mL DNAse I. Cells were lysed by homogenization and lysates clarified by centrifugation. Samples were then purified from the supernatants on Ni^{2+}-NTA Hi-Trap columns (GE Healthcare). Next, the His_6-tag was removed and samples purified further by reverse Ni^{2+}-NTA metal

affinity and size-exclusion chromatography. Proteins were then dialysed overnight in 50 mM Tris-HCl pH 8.0, 50 mM NaCl and applied to a MonoQ 5/50 GL anion exchange column (GE Healthcare) equilibrated in dialysis buffer. Finally, protein fractions were dialysed in 50 mM Tris-HCl pH 7.4, 100 mM NaCl and concentrated to 20 mg/mL. Co-expression of telethonin and Z1Z2 proteins (Z1Z2^{wt}, Z1Z2^{RGD}, Z1Z2^{Fn}) was performed in *E. coli* BL21 cells. Purification of the complexes followed the same protocol as Z_{1212}.

ZT substrate assembly

A 3:1 molar excess of telethonin to Z_{1212} (or variants) was dialysed in lysis buffer under sterile conditions using Slide-A-Lyzer^{TM} MINI dialysis device (Thermo Fisher Scientific). After dialysis equilibrium, samples were allowed to assemble at room temperature for one week before use and were subsequently stored at 4°C for up to three months.

Transmission electron microscopy

Freshly glow-discharged 400 mesh carbon-coated copper-palladium grids were incubated with diluted sample, washed with distilled water and stained with 2% uranyl acetate. All imaging was performed on a FEI 120 kV Tecnai G2 Spirit BioTWIN microscope operating at 120 kV (Biomedical Electron Microscopy Facility, University of Liverpool).

Z_{1212}^{RGD} crystal structure determination

Purified Z_{1212}^{RGD} at 15 mg/mL was crystallised using an automated nanovolume-dispensing crystallisation robot (Innovadyne Screenmaker 96+8) in 96-well Intelli-plates (Art Robbins Instruments). Crystals grew at 22°C from sitting drops containing equal volumes (100 nL) of protein and reservoir solutions (10% [w/v] 8,000 kDa polyethylene glycol, 100 mM Tris-HCl pH 7.0, 200 mM MgCl$_2$). Crystals were cryoprotected with mother liquor supplemented with

30% [v/v] glycerol prior to vitrification in liquid nitrogen. X-ray diffraction data was collected on beamline I03 (Diamond Light Source, Didcot, UK) and processed using XDS/XSCALE.[3] Molecular replacement was conducted in Phaser[4] using Z1 and Z2 domains as individual search models (PDB: 2A38[5]). Model refinement was carried out in PHENIX[6] and manual building used Coot[7]. X-ray data and model statistics are given in **Table S1**.

SEC-MALLS

SEC-MALLS measurements were acquired on an ÄKTA pure system (GE Healthcare) linked to an 8-angle light scattering detector and a differential refractometer (Helios DAWN8+ and Optilab T-rEX, Wyatt Technology). A Superdex 200 Increase 10/300 GL column (GE Healthcare) equilibrated in 50 mM Tris pH 7.4, 100 mM NaCl was used at a flow rate of 0.75 mL/min and 100 µL samples were injected at a concentration of 0.6 mg/mL. A bovine serum albumin sample (Sigma-Aldrich) was used as standard to establish detector delay volumes. Data analysis and MM calculations used the ASTRA 6.1 software suite (Wyatt Technology).

Protein adsorption to polystyrene surfaces

Solutions of sterile ZT variants, human plasma fibronectin (Merck Millipore) or truncated recombinant vitronectin (VTN-N; Gibco) were diluted in culture-grade PBS without Ca^{2+}/Mg^{2+} (Sigma Aldrich) to achieve concentrations ranging from 0.1-20 µg/mL. Proteins were passively adsorbed onto non-tissue culture treated multi-well plates (Greiner) or 8-well µ-Slides (ibidi) by adding 150 µL protein solution/cm^2 of growth area and incubating at 37°C for 2h. The protein solution was then removed and wells were immediately filled with the required medium prior to cell seeding. Unless otherwise stated, a coating concentration of 10 µg/mL was routinely used.

Cell culture

D1 murine MSCs (mMSCs) (ATCC) were cultured in Dulbecco's Modified Eagle Medium (DMEM, Sigma-Aldrich) containing 10% [v/v] foetal calf serum (Gibco), non-essential amino acids (Sigma-Aldrich), 2 mM L-glutamine (Invitrogen) and 55 µM β-mercaptoethanol (Gibco). Cells were subcultured at ~90% confluence and used up to passage number 30. For culture on ZT assemblies, mMSCs were washed twice with PBS and placed in serum-free medium (Advanced DMEM (Gibco), 100 U/mL Penicillin-Streptomycin (Invitrogen), 2 mM L-glutamine and 55 µM β-mercaptoethanol) 24h before seeding. HUES7 cells (Harvard University, HUES cells facility, Melton Laboratory, MA, USA) were cultured in serum-free mTeSR™1 medium (Stem Cell Technologies) on Matrigel (Corning). For routine expansion, cells were passaged at a 1:6 ratio on tissue culture plastic plates precoated with Matrigel according to the manufacturer's protocol. Colonies were detached from the plates with Gentle Cell Dissociation Reagent (Stem Cell Technologies) and carefully scraped/triturated to generate smaller aggregates that were passaged in fresh mTeSR™1 medium (clump passaging). Medium was exchanged daily. Cultures throughout this study did not contain ROCK inhibitor.

Cell adhesion assays

mMSCs cultured under standard conditions were serum-starved for 24h post-seeding on ZT polymers; medium was removed and the cells washed twice with phosphate-buffered saline (PBS; Sigma-Aldrich) to remove remaining serum components before serum-free medium was added. Serum-free medium was composed of Advanced DMEM (Gibco), 100 U/mL Penicillin-Streptomycin (Invitrogen), 2 mM L-glutamine and 55 µM β-mercaptoethanol. After 24h, serum-free medium was removed and cells washed once with PBS before trypsinising to generate a single cell suspension. The suspension was diluted 1:1 with serum-free medium and

centrifuged at 200 g for 3 min to pellet the cells, and the supernatant was discarded. The cells were resuspended in fresh serum-free medium and centrifugation repeated to remove residual trypsin. Finally, the cells were resuspended in serum-free medium, counted using a haemocytometer and seeded at 1×10^4 cells/cm^2 in non-TCT plates precoated with proteins. HUES7 cells cultured on Matrigel were washed once with PBS and disaggregated by incubation with Accutase (Innovative Cell Technologies) at 37°C until all cells in colonies appeared rounded and began to lift from the dish (approx. 5 min). Cells were completely detached by shear force and the suspension was diluted 1:1 with mTeSR^{TM}1 medium followed by centrifugation at 200 g for 3 min. The supernatant was removed and the pellet resuspended in fresh medium by gentle trituration to generate a single cell suspension. Seeding on protein-coated wells was as described for mMSCs, with the exception that mTeSR^{TM}1 medium was used and Matrigel was also included as an additional control. At specific time points post-seeding, mMSC and HUES7 cells were fixed with 4% [w/v] paraformaldehyde (PFA) for 10 min to halt adhesion/spreading and wells were washed with PBS to remove non-attached cells prior to analysis. For quantification, phase contrast micrographs were acquired in 3 random fields of view per well (triplicate wells, $n = 3$) using a Leica DM2500 inverted microscope and Leica DFC420C camera. Adhered cells in each field of view were counted and the average number for each condition calculated.

Proliferation assays

For hESC proliferation assays, HUES7 cells were seeded at a density of 2.5×10^3 cells/well into 96-well suspension culture plates (Greiner) coated with Matrigel, fibronectin or ZT^{Fn} (10 µg/mL). Cell number was inferred every 24h for 4 days using Cell Proliferation Reagent WST-1 (Sigma-Aldrich); following WST-1 addition, plates were incubated for 4h at 37°C and A$_{440}$ was measured using a FLUOstar Omega microplate reader (BMG LabTech). For optimisation

of protein coating concentrations, HUES7 cells were seeded at a density of 3×10^5 cells/well into 96 well suspension culture plates (Greiner) precoated with fibronectin or ZT^{Fn} at concentrations: 0.1, 0.5, 1, 2.5, 5, 10 and 20 µg/mL. Plates were incubated for 2h at 37°C, after which the wells were washed twice with PBS and WST-1 reagent was added. The plates were incubated for 4h at 37°C and A_{440} was measured at described above.

Analysis of cell morphology

For quantifying cell area, circularity, aspect ratio (AR) and solidity, individual cells were outlined using ImageJ.[8] Images were spatially calibrated (µm/pixel) and parameters calculated as follows:

$$Circularity = \frac{4\pi A}{p^2}$$

where A and p represent cell area and perimeter, respectively;

$$Solidity = \frac{A}{CA}$$

where A and CA represent area and convex area, respectively;

$$Aspect\ ratio = \frac{LA}{SA}$$

where LA and SA are the long and short axis of the best-fitted ellipsoid, respectively.

For each independent experiment, cells ($n = 50$) were measured for each condition. There where the number of observable cells was less than 50, all attached cells were measured in the images available.

Live cell imaging and migration assay

For time-lapse microscopy studies, cultures were transferred to a Cell-IQ imaging system (CM Technologies) and maintained for the duration of the experiment at 37°C and 5% CO_2. Imaging cycles were initiated 1h after cell seeding in 24 well suspension culture plates coated with protein substrates. For each condition, three random areas were imaged in triplicate wells using a 10x objective (field of view = 800 μm^2). Phase contrast images were acquired once every 15 min over 24h and data was processed using Imagen analysis software (CM Technologies).

Peptide inhibition assay

Peptide inhibition experiments followed the same protocol as cell adhesion assays. Following trypsinisation, mMSCs were incubated with 0, 2.5, 25 or 250 µM of integrin-binding GRGDS or 250 µM control GRGES pentapeptides (Protein Peptide Research Fareham, UK) for 15 minutes. Cells were then seeded in suspension culture plates coated with control fibronectin or ZT assemblies at 10 µg/mL. After 2h incubation at 37°C, cells were fixed with 4% PFA [w/v] for 10 min at room temperature and imaged by phase contrast microscopy as described above.

Maintenance of human embryonic stem cell pluripotency

HUES7 cells cultured on Matrigel were detached using the clump passaging procedure and seeded onto suspension culture plates (Gibco) coated with fibronectin or ZT[Fn] assemblies at 10 µg/mL. Once confluent, cells were passaged onto fresh substrates using the same method and fixed as above after five or ten passages for analysis by immunofluorescence.

Clonogenic assays

Suspensions of single HUES7 cells were generated with Accutase and seeded at a density of $2.5 \times 10^3/cm^2$ on 12 well suspension culture plates coated with protein substrates. Cells were

cultured for 4 days under standard conditions and fixed with 4% [w/v] PFA before staining with 0.1% [w/v] crystal violet. The number of colonies per well was calculated using the Analyse Particles function of ImageJ.[8]

Embryoid body formation

HUES7 cells grown on fibronectin or ZT^{Fn} for thirteen passages were dissociated with Accutase to generate a single cell suspension. Cells were resuspended in STEMdiff^{TM} APEL^{TM} Medium (Stem Cell Technologies) and plated at 3000 cells per well in 96-well round bottom Nunclon^{TM} Sphera^{TM} Microplates (Thermo Scientific). To promote aggregation, plates were centrifuged at 140 g for 2 mins and incubated at 37°C with 5% CO_2 to allow embryoid bodies to develop. Following 10 days of culture, embryoid bodies were transferred to Matrigel-coated 8-well chamber slides and allowed to attach for a further 10 days in STEMdiff^{TM} APEL^{TM} Medium prior to fixation (as above). Next, staining for germ layer derivatives was carried out using antibodies against Brachyury, GATA6, and Nestin (described below) and visualisation proceeded by confocal microscopy.

Real-time quantitative polymerase chain reaction (RT-qPCR)

HUES7 cells cultured on different substrates were lysed with TRI Reagent (Sigma) and RNA was extracted according to the manufacturer's protocol. For cDNA synthesis, RNA was first treated with DNase 1 (Promega) and reverse transcribed using random hexamers (Qiagen) and Superscript III (Invitrogen). Real-time quantitative PCR analysis was performed on a Bio-Rad CFX Connect system using SYBR Green JumpStart Taq ReadyMix (Sigma). Gene expression was normalised using the geometric mean C_T values for reference genes *GAPDH and HPRT1*. Relative expression of target genes between cells grown on fibronectin or ZT^{Fn} for multiple passages and control cells on Matrigel used the $2^{-\Delta\Delta Ct}$ method.[9] Primer sequences (5'–3') were

as follows: GAPDH F-GTGGAAGGACTCATGACCA, R-GAGGCAGGGATGATGTTCT; HPRT1 F-GCAGCCCTGGCGTCGTGATTAG, R-TCGAGCAAGACGTTCAGTCCTGTCC; NANOG F-TCCAACATCCTGAACCTCAGC, R-GAGGCCTTCTGCGTCACA; OCT4 F-ATGTGGTCCGAGTGTGGTTC, R-TGTGCATAGTCGCTGCTTGA; SOX2 F-TCAGGAGTTGTCAAGGCAGAG, R-GGCAGCAAACTACTTTCCCC.

Staining using immunocytochemistry

For confocal microscopy, cells were seeded in untreated plastic 8-well µ-Slides (Ibidi) coated with substrates at 10 µg/mL. After 4h incubation, cells were washed twice with PBS, fixed with 4% [w/v] PFA for 10 mins, permeabilised with 0.1% Triton X-100 for a further 10 min and blocked with 1% [w/v] BSA for 30 mins before application of primary antibodies. For immunofluorescence, all primary antibodies were incubated overnight at 4°C followed by secondary antibody application for 2h at room temperature (RT). Primary antibodies for focal adhesion and integrin staining were as follows; rabbit anti-paxillin (Abcam ab32084), rabbit anti-FAK phospho Y397 (Abcam ab39967), rat anti-α5 subunit (mAb11[10]), mouse anti-αV subunit (L230 ATCC), mouse anti-αVβ3 integrin (MAB1976 Merck Millipore), rabbit anti-β5 subunit (Cell Signaling Technology 3629) and rabbit anti-β1 subunit (Abcam ab52971). For pluripotency and differentiation markers, HUES7 cells were probed with mouse anti-OCT3/4 (Santa Cruz Biotechnology sc-5279), rabbit anti-NANOG (Cell Signaling Technology D73G4), rabbit anti-GATA6 (Santa Cruz Biotechnology sc-9055), rabbit anti-Nestin (Abcam ab92391) and goat anti-Brachyury (Santa Cruz Biotechnology sc-17743) primary antibodies. Secondary antibodies were goat anti-rabbit AlexaFluor594, goat anti-mouse AlexaFluor594, donkey anti-goat AlexaFluor488, chicken anti-rabbit AlexaFluor488/594 and chicken anti-rat AlexaFluor488 (Invitrogen). All secondary antibodies were used at 1:1000 dilutions.

Observation of F-actin filaments used AlexaFluor488 Phalloidin (Invitrogen) and cell nuclei were counterstained with 4',6-diamino-2-diamino-2-phenylindole, dilactate (DAPI; Invitrogen). Imaging was conducted on a 3i Spinning Disk confocal microscope with a Zeiss autofocus system and Hamamatsu camera using 20x air or 40x and 63x oil objectives.

Statistical analysis

All cell-based measurements were repeated a minimum of three times and their statistical significance determined by two-sample unpaired Student's t-test using Minitab 17 software (www.minitab.com). Statistical significance was inferred when $p<0.05$ (*), highly significant when $p<0.01$ (**) and very highly significant when $p<0.001$ (***).

Figure S1

Fig. S1. Characterisation of protein chimeras and Z1Z2/Tel complexation following functionalisation. (**A**) Size-exclusion chromatogram overlays of Z_{1212} (solid line), Z_{1212}^{RGD} (dashed line) and Z_{1212}^{RGE} (dotted line) (Superdex 200 16/60 column; GE Healthcare). Sample purity was evaluated by SDS-PAGE (inset). Coincident exclusion profiles indicate that the modification of the Z_{1212} tandem did not cause undesirable fold alterations. (**B**) Size-exclusion chromatogram overlays of Z_{1212} (solid line) and Z_{1212}^{Fn} (dashed line). Sample purity was evaluated by SDS-PAGE (inset). (**C**) SEC-MALLS profiles of Z_{1212}^{RGD} (black) and Z_{1212}^{Fn} (red) fractionated on a Superdex 200 Increase 10/300 GL column (GE Healthcare). The average MM per volume unit (horizontal line) is plotted against the normalised differential refractive index. Experimental values (MM_{exp}) and values calculated from sequence data (MM_{calc}) are given. The data show that the modified samples retain their monomeric and monodisperse character. (**D**) Elution profile overlays for $Z1Z2^{WT}$-Tel (solid line), $Z1Z2^{RGD}$-Tel (dashed line) and $Z1Z2^{Fn}$-Tel (dotted line) complexes. Schematic representations of complexes are shown to the left or right of their corresponding peaks. The data prove that the functional moieties introduced do not impair the binding of Z_{1212} and Tel components. (**E**) SEC-MALLS analysis of $Z1Z2^{RGD}$-Tel (black) and $Z1Z2^{Fn}$-Tel (red) complexes. The average MM per volume unit (horizontal line) is plotted against the normalised differential refractive index. Experimental values (MM_{exp}) and values calculated from sequence data (MM_{calc}) are given. Measured MM values confirm that complexes retain their monodispersity and that the totality of the sample is in the assembled state. (**F**) Native-PAGE profiles of ZT polymers and corresponding Z_{1212} tandem variants 24 h post-assembly. (**G**) Native-PAGE profiles of ZT^{Fn} and Z_{1212}^{Fn} compared to wild type ZT polymer and Z_{1212} tandem.
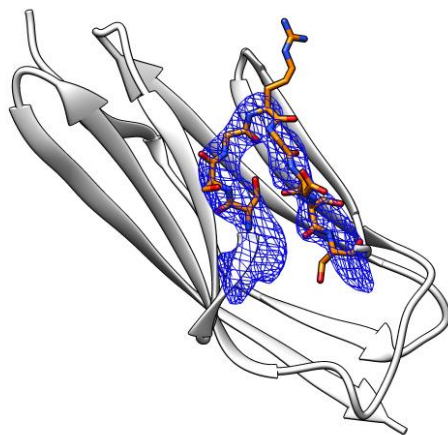
**Fig. S2. Electron density omit map of the engineered CD loop**

(2Fo-Fc)αc electron density map (contoured at 1σ) of the engineered CD loop in Z1 (shown

as sticks in orange) The map was calculated upon omitting the loop from the model, so that

no model was present in that location.
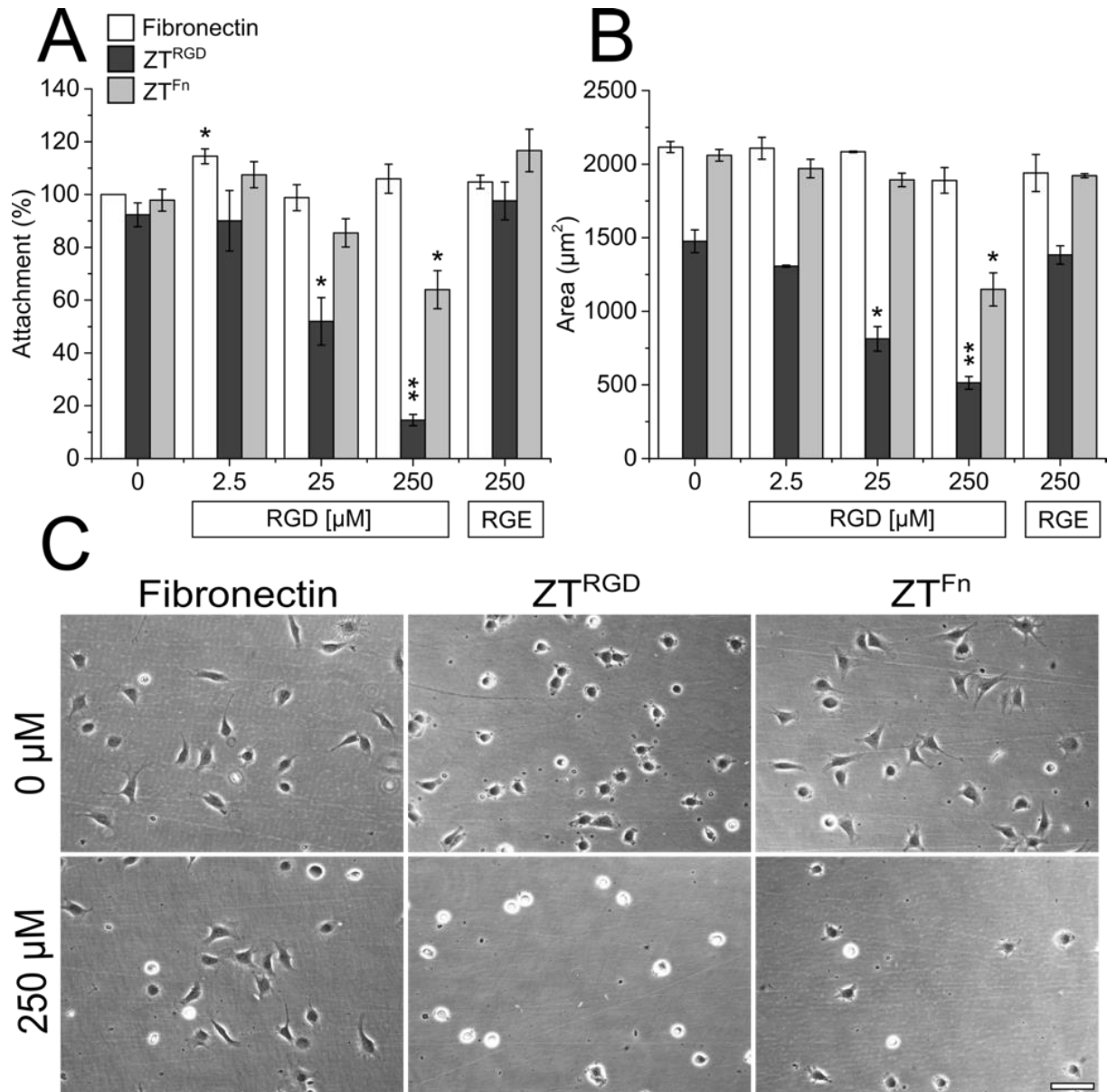
Fig. S3. Inhibition of cell attachment and spreading by the GRGDS pentapeptide.
Quantification of cell attachment (**A**) and spreading (**B**) on fibronectin, ZT^{RGD} and ZT^{Fn} in the
presence of GRGDS and GRGES (control) peptides. Significant differences between untreated
(0 µM) and peptide-treated groups are marked with asterisks (*$p < 0.05$ and **$p < 0.01$). Error
bars represent SEM ($n = 4$ and $n = 3$ for attachment and area, respectively). (**C**) Representative
micrographs illustrating the effect of 250 µM integrin-binding peptide on mMSC adhesion to
fibronectin, ZT^{RGD} and ZT^{Fn} (all samples adsorbed at 10 µg/mL). Scale bar = 100 µm.
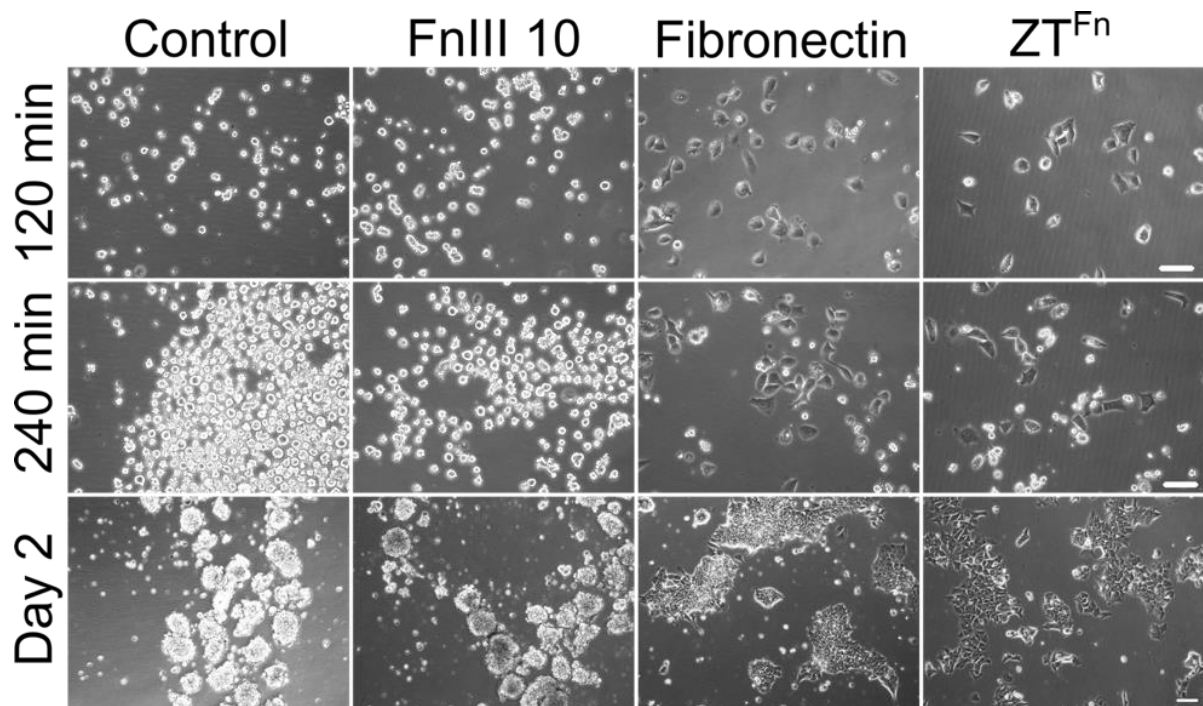
Fig. S4. Effect of domain Fn10 respect to ZT^{Fn} and fibronectin substrates on hESC attachment and spreading. Representative phase-contrast micrographs of HUES7 cells on different substrates at 2, 4 and 48 h post-seeding. Proteins were passively adsorbed onto non-tissue culture treated 24-well plates at a coating concentration of 10 µg/mL. The control consisted of PBS alone. Scale bars = 100 µm.
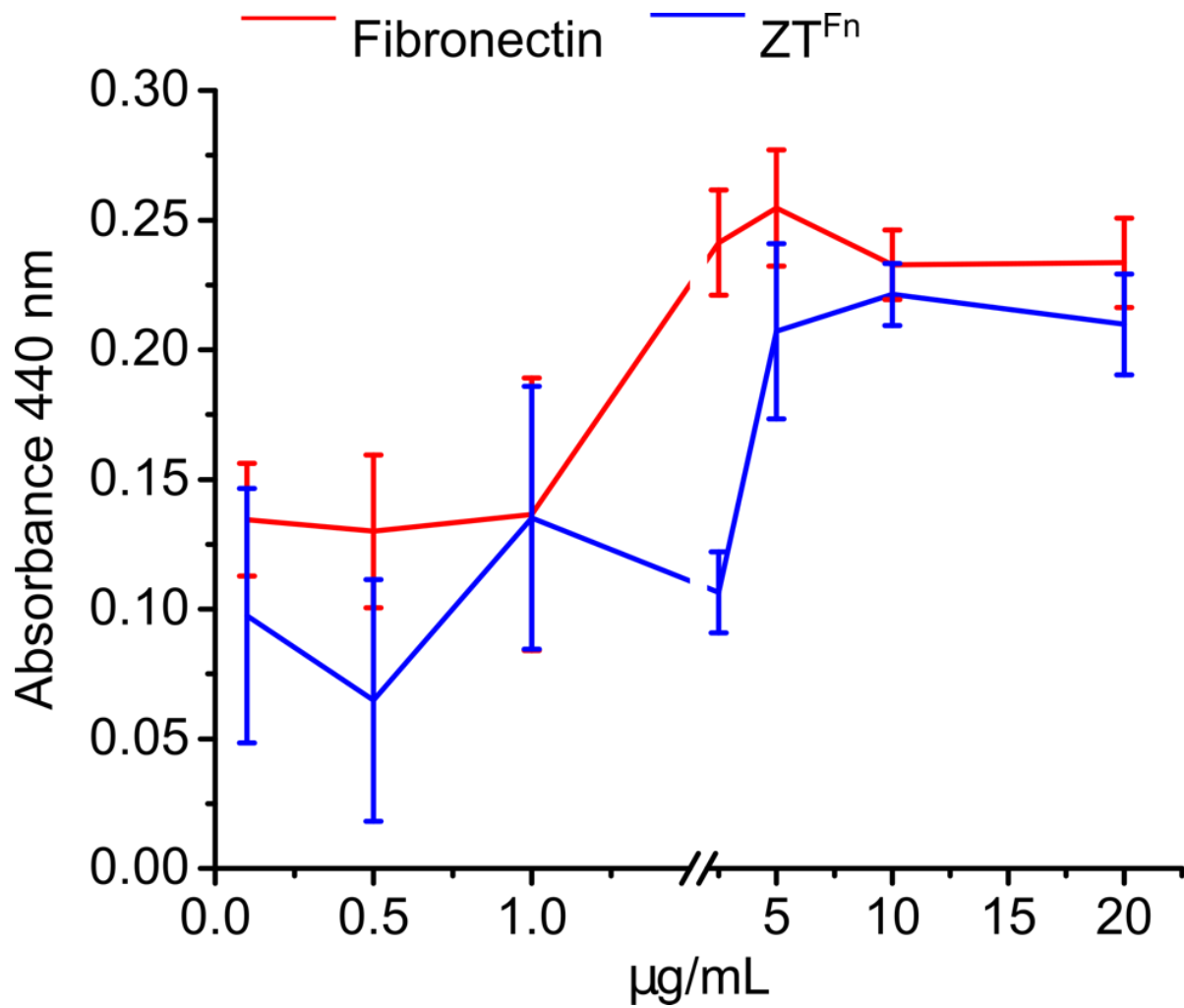
Fig. S5. Concentration-dependent attachment of hESCs to protein substrates. HUES7 cells were seeded onto fibronectin or ZT^{Fn} coated surfaces at the indicated concentrations and allowed to attach for 2 hours. The extent of cell attachment was measured using WST-1 reagent. Error bars represent SEM ($n = 3$).
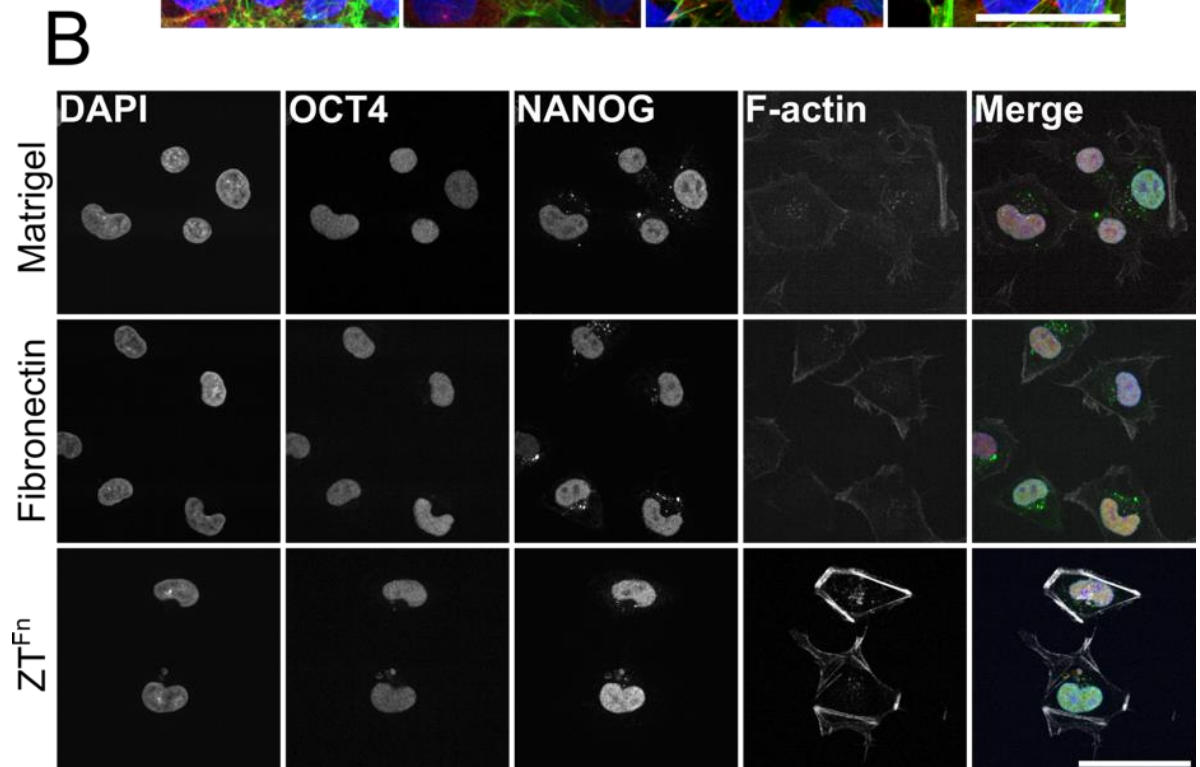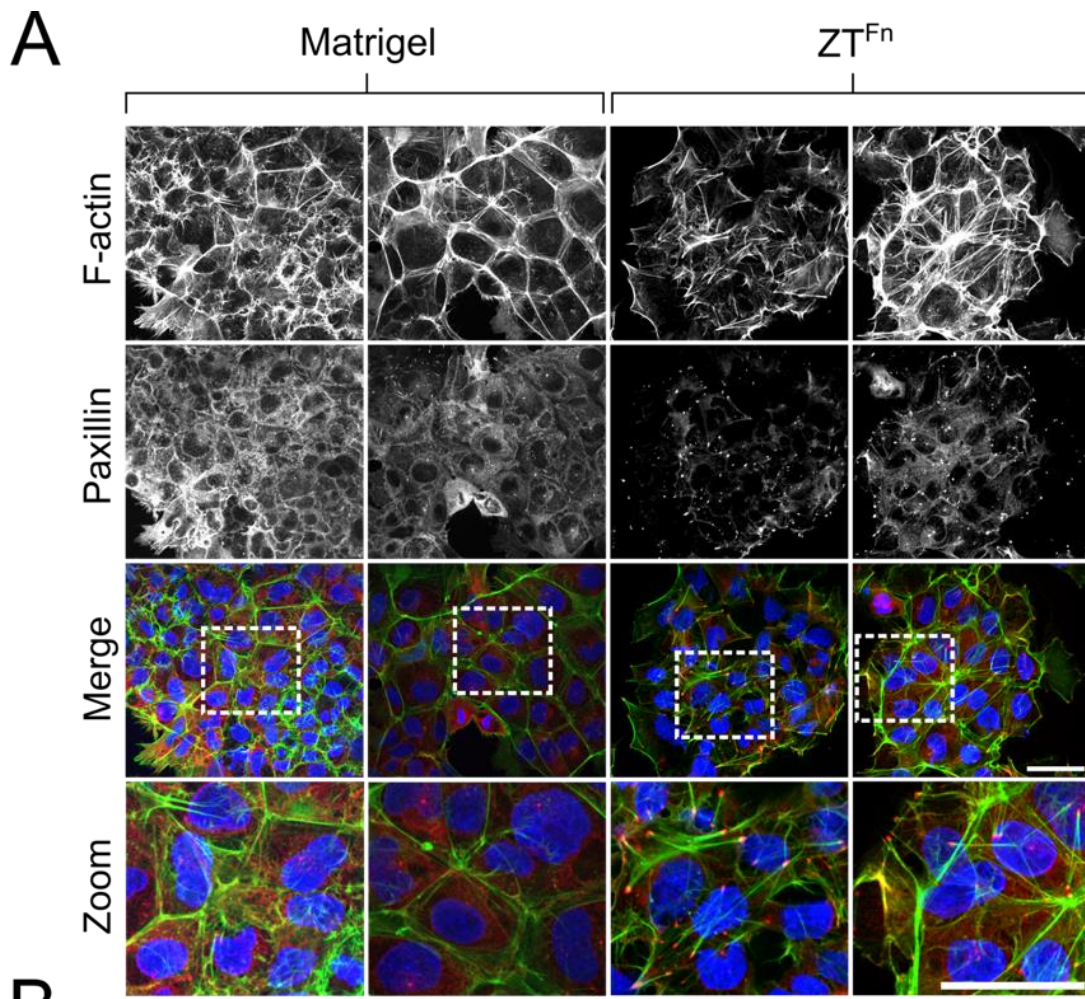
Fig. S6. Colony morphology and expression of pluripotency markers in HUES7 cells. (**A**) Representative confocal micrographs of HUES7cells cultured on Matrigel or ZT^{Fn} for 2 days and stained for F-actin (green) and paxillin (red). The lower panels show merged channel images with DAPI counterstaining (blue) and zooms of boxed areas. Scale bars = 50 μm. (**B**) Images show HUES7 cells following 4 h attachment on Matrigel, fibronectin or ZT^{Fn} and stained for nuclei (blue), OCT4 (red), NANOG (green) and F-actin (white). Merged channel images are shown to the right. Scale bar = 50 μm.
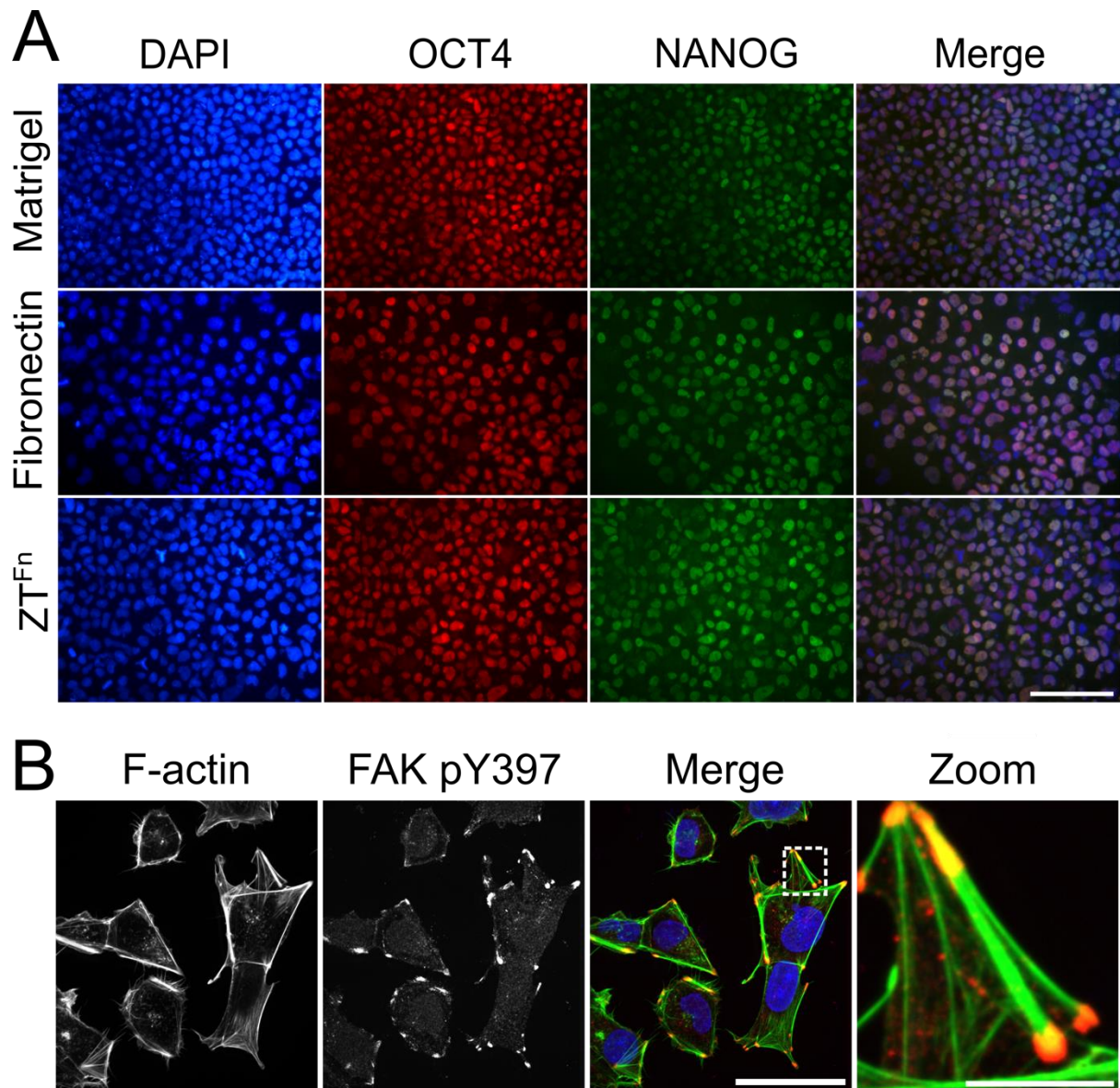
Fig. S7. Expression of pluripotency markers and focal adhesion kinase activation. (**A**) Immunofluorescence micrographs show HUES7 cells stained for nuclei (blue), OCT4 (red) and NANOG (green) following 7 d culture on protein substrates. Scale bar = 100 μm. (**B**) Representative confocal micrograph of HUES7 cells cultured on ZT^{Fn} and stained for F-actin (green) and FAK pY397 (red). The merged channel image includes DAPI counterstaining (blue) and a zoom of the boxed area is shown to the right. Scale bars = 50 μm and 10 μm.
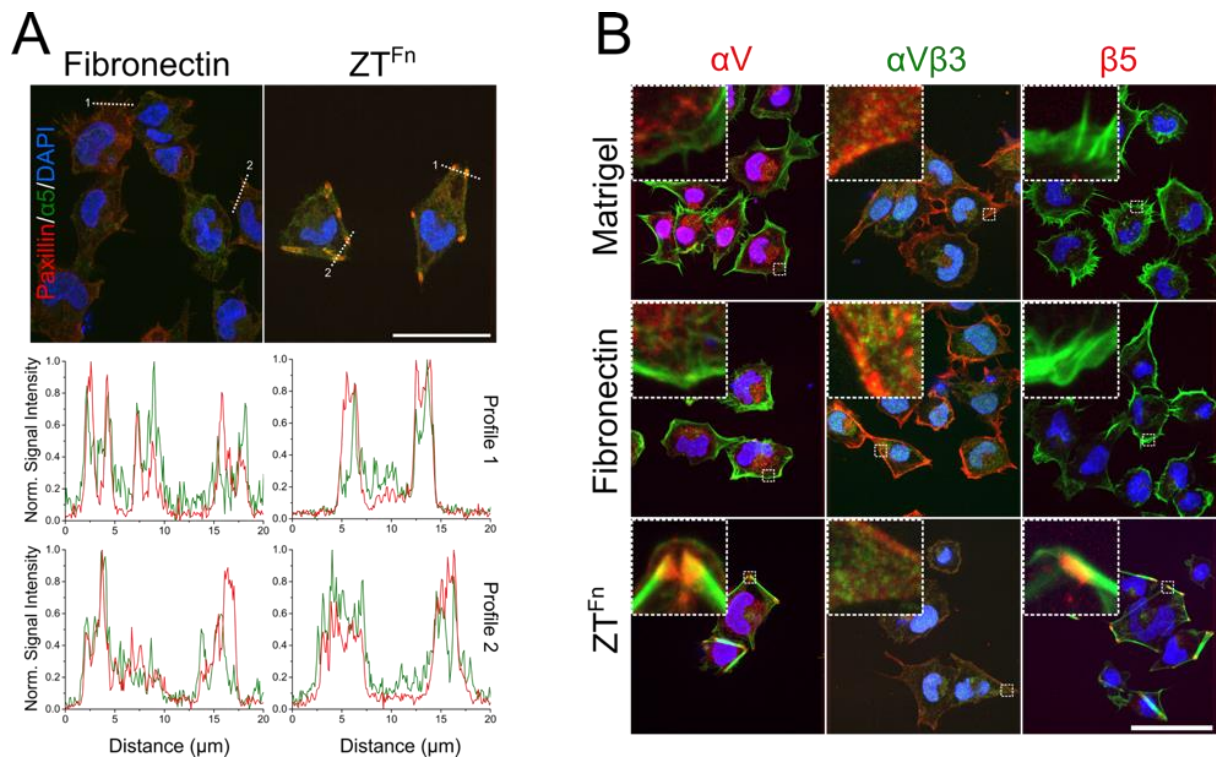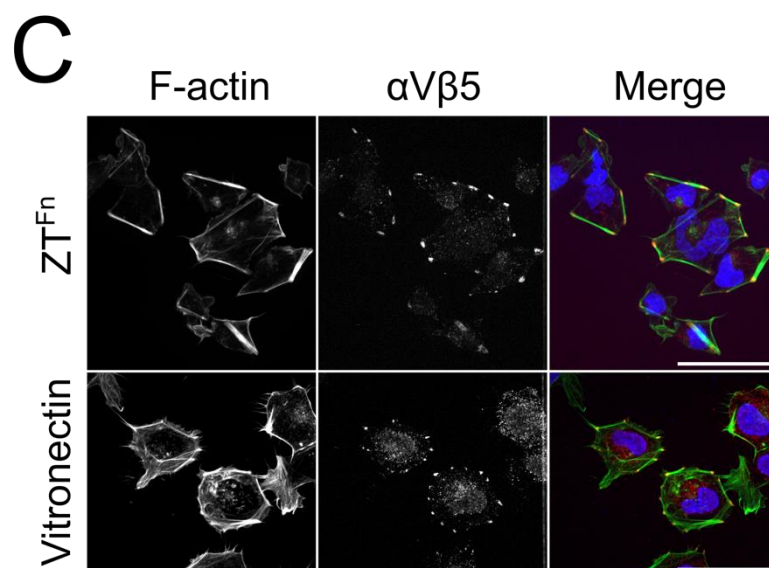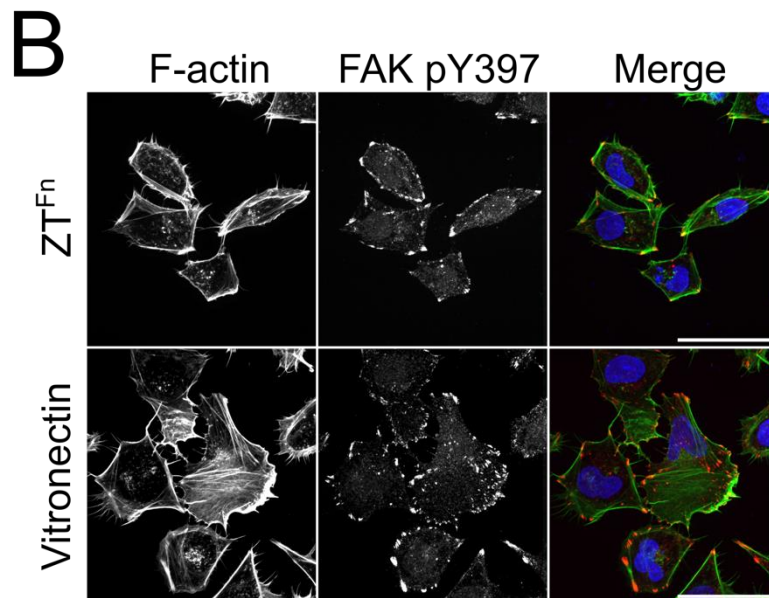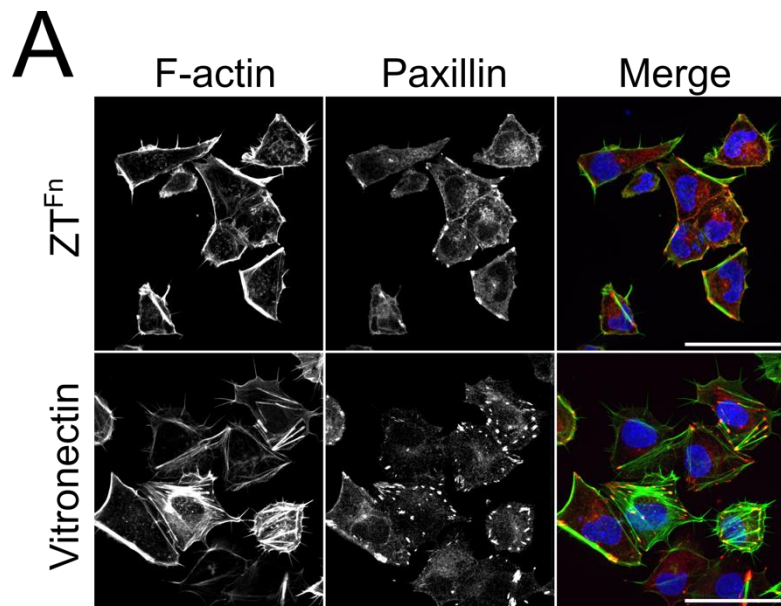
Fig. S8. Integrin engagement in human ESCs plated on protein substrates. (**A**) Top panels show representative confocal micrographs of HUES7 cells following 4h culture on fibronectin or ZT^{Fn} and co-stained for paxillin (red), α5β1 (green) and nuclei (blue). Fluorescence intensity line scan profiles for paxillin and α5β1 are shown below the respective micrographs. The strong correlation observed between paxillin and α5β1 localisation supports engagement of this integrin on fibronectin and ZT^{Fn} substrates. (**B**) HUES7 cells stained for integrin αV subunit (red), αVβ3 heterodimer (green) or β5 subunit (red) following 4h attachment to protein substrates. Cells were counterstained with phalloidin and DAPI (blue). Zooms of the boxed areas are shown in the upper left corner of each image. Scale bars = 50 µm.
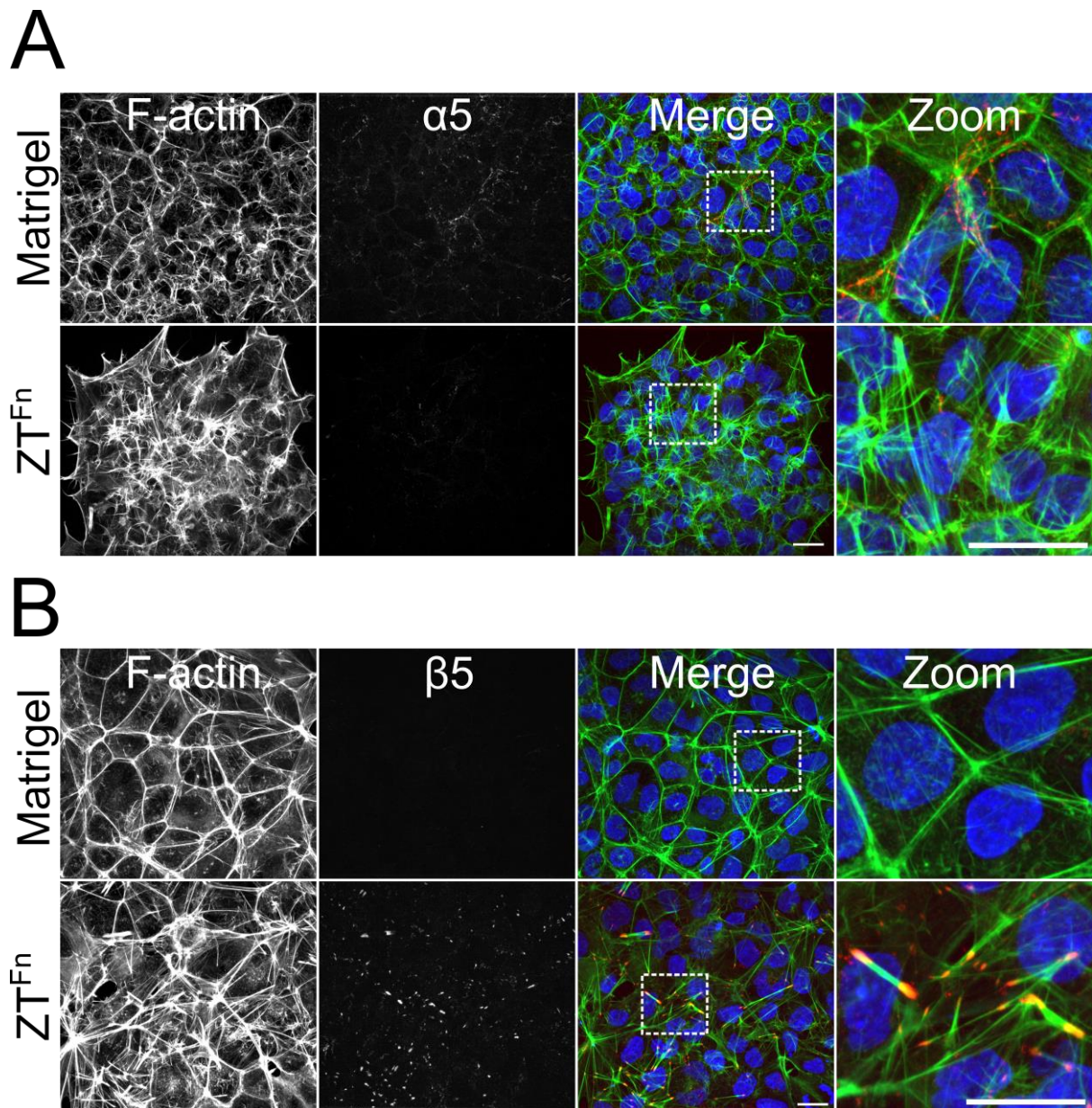
Fig. S9. Human ESC-matrix interactions on Matrigel and ZT^{Fn} following 2 days of culture. Representative immunofluorescence micrographs show staining of HUES7 cells for α5 integrin subunit (**A**: red) or β5 integrin subunit (**B**: red) Cells were counterstained with phalloidin (green) and DAPI (blue). Zooms of merged channel images are shown on the right of each panel. Scale bars = 25 μm.

A

F-actin   Paxillin   Merge

ZT^Fn

Vitronectin

B

F-actin   FAK pY397   Merge

ZT^Fn

Vitronectin

C

F-actin   αVβ5   Merge

ZT^Fn

Vitronectin

Fig. S10. Comparison of human ESC morphology and focal adhesion complexes when cultured on ZT^{Fn} or vitronectin. Representative immunofluorescence micrographs show HUES7 cells following 4h culture on vitronectin or ZT^{Fn} and stained for paxillin (**A**: red), FAK pY397 (**B**: red) and αVβ5 integrin (**C**: red). Cells were counterstained with phalloidin (green) and DAPI (blue). Scale bars = 50 μm.
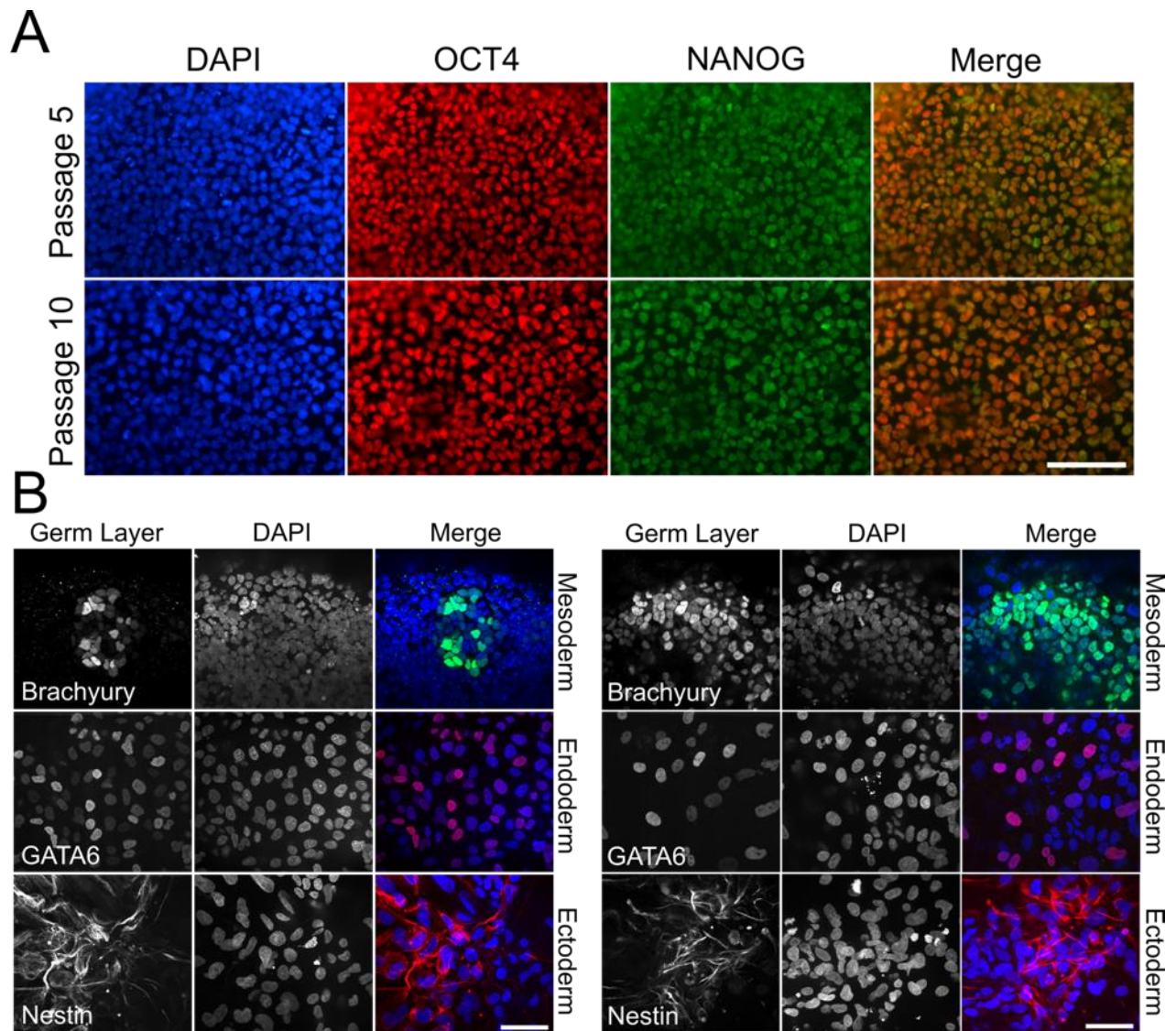
Fig. S11. Human ESC self-renewal and maintained pluripotency on ZT^{Fn}. (**A**) Immunofluorescence micrographs show HUES7 cells stained for nuclei (blue), OCT4 (red) and NANOG (green) following five or ten passages on ZT^{Fn}. Scale bar = 100 μm. (**B**) HUES7 cells cultured fibronectin (left panels) or ZT^{Fn} (right panels) for thirteen passages were used to form embryoid bodies which were subsequently allowed to attach and spread on Matrigel. Representative confocal micrographs show embryoid body-derived cells stained for markers of the three primary germ layers; Brachyury (green), GATA6 (red) and Nestin (red). Cells were counterstained with DAPI (blue). Scale bar = 50 μm.

Table S1. Data collection and refinement statistics.

Space group	H3
Cell dimensions (Å)	$a = 133.4$ $b = 134.4$ $c = 134.0$ $\alpha = 90.00$ $\beta = 90.00$ $\gamma = 120.00$
Diffraction data	
Beamline	I03 (Diamond Light Source)
Detector	Pilatus3 6M
Wavelength (Å)	0.97
Resolution (Å)	41.8 – 3.0 (3.108 – 3.0)
Unique reflections	17993 (1813)
R_{merge}(I)	0.1087 (1.803)
Multiplicity	4.1 (4.0)
Completeness (%)	0.99 (1.00)
I/σ(I)	9.26 (0.60)
$CC_{1/2}$	0.996 (0.162)
Refinement	
Reflections in working/free set	73091 / 910
Number of protein residues	390
R-factor/R-free (%)	19.2 / 22.4
RMSD bond length (Å)/bond angle (°)	0.002 / 0.5
Ramachandran plot favoured/allowed/outliers (%)	97.1 / 2.4 / 0.5

Movie S1. Dissociated HUES7 cells cultured on Matrigel at a density of 10×10^3 cells/cm^2. Phase-contrast images were acquired every 15 min for 24 h. Scale bar = 200 μm.

Movie S2. Dissociated HUES7 cells cultured on fibronectin at a density of 10×10^3 cells/cm^2. Phase-contrast images were acquired every 15 min for 24 h. Scale bar = 200 μm.

Movie S3. Dissociated HUES7 cells cultured on ZT^{Fn} at a density of 10×10^3 cells/cm^2. Phase-contrast images were acquired every 15 min for 24 h. Scale bar = 200 μm.

References

[1] M. Bruning, L. Kreplak, S. Leopoldseder, S. A. Muller, P. Ringler, L. Duchesne, D. G. Fernig, A. Engel, Z. Ucurum-Fotiadis, O. Mayans, *Nano Lett.* **2010**, *10*, 4533.

[2] J. Braman, C. Papworth, A. Greener, *Methods Mol. Biol.* **1996**, *57*, 31.

[3] W. Kabsch, *Acta Crystallogr. Sect. D Biol. Crystallogr.* **2010**, *66*, 125.

[4] A. J. McCoy, R. W. Grosse-Kunstleve, P. D. Adams, M. D. Winn, L. C. Storoni, R. J. Read, *J. Appl. Crystallogr.* **2007**, *40*, 658.

[5] M. Marino, P. Zou, D. Svergun, P. Garcia, C. Edlich, B. Simon, M. Wilmanns, C. Muhle-Goll, O. Mayans, *Structure* **2006**, *14*, 1437.

[6] P. D. Adams, P. V. Afonine, G. Bunkóczi, V. B. Chen, I. W. Davis, N. Echols, J. J. Headd, L. W. Hung, G. J. Kapral, R. W. Grosse-Kunstleve, A. J. McCoy, N. W. Moriarty, R. Oeffner, R. J. Read, D. C. Richardson, J. S. Richardson, T. C. Terwilliger, P. H. Zwart, *Acta Crystallogr. Sect. D Biol. Crystallogr.* **2010**, *66*, 213.

[7] P. Emsley, B. Lohkamp, W. G. Scott, K. Cowtan, *Acta Crystallogr. Sect. D Biol. Crystallogr.* **2010**, *66*, 486.

[8]   C. a Schneider, W. S. Rasband, K. W. Eliceiri, *Nat. Methods* **2012**, *9*, 671.

[9]   K. J. Livak, T. D. Schmittgen, *Methods* **2001**, *25*, 402.

[10]   S. Miyamoto, S. K. Akiyama, K. M. Yamada, *Science* **1995**, *267*, 883.